

TR-534
**Design Procedures and Field Monitoring of Submerged Barbs for
Streambank Protection**

FINAL REPORT



Submitted to:
Iowa Department of Transportation, Highway Division
Iowa Highway Research Board
800 Lincoln Way
Ames, Iowa, 50010

Submitted by:
Prof. Thanos Papanicolaou
Co-author: Dr. Mohamed Elhakeem
IIHR-Hydrosience & Engineering
College of Engineering
The University of Iowa
Iowa City, Iowa 52242



June 2007

About the IIHR- Hydroscience & Engineering

IIHR, a unit of The University of Iowa's College of Engineering, is one of the nation's premier and oldest fluids research and engineering laboratories. Situated on the Iowa River in Iowa City, Iowa, IIHR seeks to educate students and to conduct research in the broad fields of hydraulics and fluid mechanics.

Disclaimer Notice

The contents of this report reflect the views of the authors, who are responsible for the facts and the accuracy of the information presented herein. The opinions, findings and conclusions expressed in this publication are those of the authors and not necessarily those of the sponsors.

The sponsors assume no liability for the contents or use of the information contained in this document. This report does not constitute a standard, specification, or regulation.

The sponsors do not endorse products or manufacturers. Trademarks or manufacturers' names appear in this report only because they are considered essential to the objective of the document.

Non-discrimination Statement

The University of Iowa does not discriminate on the basis of race, color, age, religion, national origin, sexual orientation, gender identity, sex, marital status, disability, or status as a U.S. veteran. Inquiries can be directed to the Director of Equal Opportunity and Diversity at the University of Iowa, (319) 335-0705.

Technical Report Documentation Page

1. REPORT NO. IHRB Project TR-534		2. GOVERNMENT ACCESSION NO.		3. RECIPIENT'S CATALOG NO.	
4. TITLE AND SUBTITLE Design Procedures and Field Monitoring of Submerged Barbs for Streambank Protection				5. REPORT DATE June 2007	
				6. PERFORMING ORGANIZATION CODE	
7. AUTHOR(S) A.N. Thanos Papanicolaou, Mohamed Elhakeem				8. PERFORMING ORGANIZATION REPORT NO.	
9. PERFORMING ORGANIZATION NAME AND ADDRESS IIHR- Hydrosience & Engineering The University of Iowa 300 South Riverside Drive Iowa City, Iowa 52242-1585				10. WORK UNIT NO.	
				11. CONTRACT OR GRANT NO.	
12. SPONSORING AGENCY NAME AND ADDRESS Iowa Highway Research Board Iowa Department of Transportation 800 Lincoln Way Ames, IA 50010		15. SUPPLEMENTARY NOTES This study was conducted in cooperation with the Iowa Department of Transportation		13. TYPE OF REPORT AND PERIOD COVERED Final Report	
				14. SPONSORING AGENCY CODE	
16. ABSTRACT <p>The main objective of this study was to evaluate the hydraulic performance of riprap spurs and weirs in controlling bank erosion at the Southern part of the Raccoon River upstream U.S. Highway 169 Bridge utilizing the commercially available model FESWMS and field monitoring. It was found based on a 2 year monitoring and numerical modeling that the design of structures was overall successful, including their spacing and stability. The riprap material incorporated into the structures was directly and favorably correlated to the flow transmission through the structure, or in other words, dictated the permeable nature of the structure. It was found that the permeable dikes and weirs chosen in this study created less volume of scour in the vicinity of the structure toes and thus have less risk comparatively to other impermeable structures to collapse. The fact that the structures permitted the transmission of flow through them it allowed fine sand particles to fill in the gaps of the rock interstices and thus cement and better stabilize the structures. During bank-full flows the maximum scour hole was recorded away from the structures toe and the scour-hole size was directly related to the protrusion angle of the structure to the flow. It was concluded that the proposed structure inclination with respect to the main flow direction was appropriate since it provides maximum bank protection while creating the largest volume of local scour away from the structure and towards the center of the channel. Furthermore, the lowest potential for bank erosion also occurs with the present set-up design chosen by the IDOT. About 2 ft of new material was deposited in the area located between the structures for the period extending from the construction day to May 2007. Surveys obtained by sonar and the presence of vegetation indicate that new material has been added at the bank toes. Finally, the structures provided higher variability in bed topography forming resting pools, creating flow shade on the leeward side of the structure, and separation of bed substrate due to different flow conditions. Another notable environmental benefit to rock riprap weirs and dikes is the creation of resting pools, especially in year 2007 (2nd year of the project). The magnitude of these benefits to aquatic habitat has been found in the literature that is directly related to the induced scour-hole volume.</p>					
17. KEY WORDS Key words: barbs design, erosion control, hydrodynamic models			18. DISTRIBUTION STATEMENT No restrictions.		
19. SECURITY CLASSIF. (of this report) None		20. SECURITY CLASSIF. (of this page) None		21. NO. OF PAGES	22. PRICE NA

Reproduction of completed page authorized

Design Procedures and Field Monitoring of Submerged Barbs for Streambank Protection

Final Report
June 2007

Principal Investigator

Prof. Thanos Papanicolaou
Associate Professor
IIHR - Hydroscience & Engineering
The University of Iowa
Iowa City, IA 52242

Postdoctoral Associate

Dr. Mohamed Elhakeem
IIHR-Hydroscience & Engineering
The University of Iowa
Iowa City, Iowa 52242

Sponsored by
The Iowa Highway Research Board (IHRB Project TR-534)

A report from
IIHR-Hydroscience & Engineering
College of Engineering
The University of Iowa
Iowa City, Iowa 52242
Phone: 319 335-5237
Fax: 319 335 5238
www.ihr.uiowa.edu

ACKNOWLEDGEMENTS

This study was funded by the Iowa Highway Research Board. The writers are indebted to Dave Claman from the IDOT for all the information and help that he provided during the study. The writers would like also to thank Brian Wardman for his help in running the numerical code and Dermisis Dimitrios and Achilleas Tsakiris for their help with the completion of the field work.

TABLE OF CONTENTS

	<u>Page</u>
ACKNOWLEDGEMENTS	v
TABLE OF CONTENTS	vi
LIST OF TABLES	vii
LIST OF FIGURES	viii
1. INTRODUCTION	1
2. STUDY SITE	3
3. METHODOLOGY	4
3.1 Critical Design Characteristics	5
3.2 Choice of Numerical Model	7
3.3 Sources of Model Uncertainty	9
3.4 Data Collection for Model Calibration	10
3.5 Model Calibration	12
4. MODEL BEHAVIOR AND CALIBRATION	14
4.1 Sensitivity Analysis	14
4.2 Field Measurements for Model Calibration	16
4.3 Error Analysis	20
4.4 Calibrated Model	21
4.5 Sediment Transport Measurements	22
5. RESULTS	25
6. CONCLUSIONS	34
6.1 Numerical Model Performance	34
6.2 Structure Performance	35
6.3 Environmental Benefits of Structures	35
REFERENCES	36
APPENDIX 1: External Calibration Results	38

LIST OF TABLES

	<u>Page</u>
Table 1: Summary of the flow conditions and sensitivity analysis parameters.	15
Table 2: Reattachment length for various Manning's coefficient values.	15
Table 3: Reattachment length for various eddy viscosity values.	15
Table 4: Manning's coefficient and eddy viscosity for different locations.	21

LIST OF FIGURES

	<u>Page</u>
Figure 1. Observed movement of Raccoon River Channel Upstream of the U.S. Highway 169 Bridge (Claman, 2005). The various color bands represent the observed location of the streambanks during the year indicated. U.S. Highway 169 can be seen running North and South along the right hand side of the photo. Flow is from left to right.	2
Figure 2. Typical bendway weir design as constructed at the Raccoon River study site. Picture taken from the channel center looking perpendicular at bank with flow going from left to right. The bridge (not pictured) is located downstream of this structure.	3
Figure 3. Constructed bendway weirs looking upstream from the U.S. Highway 169 Bridge.	4
Figure 4. Typical flow structure near a bendway weir (plan view).	5
Figure 5. Typical flow patterns in a groyne field (plan view): a) $S/L < 0.5$; b) $0.5 < S/L < 2.0$; and c) $S/L > 2.0$.	7
Figure 6. Computational Mesh used for model calibration. Flow is from left to right.	13
Figure 7. Simplified channel used in sensitivity analysis.	14
Figure 8. Locations of LSPIV Measurements.	17
Figure 9. LSPIV velocity measurements for $Q = 315 \text{ ft}^3/\text{s}$ flow event.	17
Figure 10. Comparison of measured and calculated values for selected transects. (Point 0 of the transect is nearest to the bank and point 20 is closest to the channel centerline).	18
Figure 11. Location of ADV measurements relative to the bendway weir.	19
Figure 12. Analysis of the measured ADV velocity components.	19
Figure 13. Comparison of calculated and measured depths.	20
Figure 14. Comparison of calculated and measured velocities.	21
Figure 15. Classification of flow resistance areas according to Manning's coefficient and eddy viscosity for the region of interest.	22
Figure 16. Deposition processes after barbs construction.	23
Figure 17. Measured deposition between two furthest upstream bendway weirs in ft.	23
Figure 18. Measured scour depth around toe of bendway weir.	24
Figure 19. Sieve analysis of bed samples collected from the field site.	24
Figure 20a. No barbs present, sand bar present, discharge (Q) = $11,000 \text{ ft}^3/\text{s}$, downstream water surface elevation (DWSE) = 869.9 ft.	26
Figure 20b. Barbs present, sand bar present, discharge (Q) = $11,000 \text{ ft}^3/\text{s}$, downstream water surface elevation (DWSE) = 869.9 ft.	26
Figure 21a. No barbs present, sand bar present, discharge (Q) = $11,000 \text{ ft}^3/\text{s}$, downstream water surface elevation (DWSE) = 869.9 ft.	27
Figure 21b. Barbs present, sand bar present, discharge (Q) = $11,000 \text{ ft}^3/\text{s}$, downstream water surface elevation (DWSE) = 869.9 ft.	27

Figure 22a. No barbs present, sand bar present, discharge (Q) = 11,000 ft ³ /s, downstream water surface elevation (DWSE) = 869.9 ft.	28
Figure 22b. Barbs present, sand bar present, discharge (Q) = 11,000 ft ³ /s, downstream water surface elevation (DWSE) = 869.9 ft.	28
Figure 23a. No barbs present, sand bar present, discharge (Q) = 11,000 ft ³ /s, downstream water surface elevation (DWSE) = 869.9 ft.	29
Figure 23b. Barbs present, sand bar present, discharge (Q) = 11,000 ft ³ /s, downstream water surface elevation (DWSE) = 869.9 ft.	29
Figure 24a. No barbs present, no sand bar present, discharge (Q) = 11,000 ft ³ /s, downstream water surface elevation (DWSE) = 869.9 ft.	30
Figure 24b. Barbs present, no sand bar present, discharge (Q) = 11,000 ft ³ /s, downstream water surface elevation (DWSE) = 869.9 ft.	30
Figure 25a. No barbs present, no sand bar present, discharge (Q) = 11,000 ft ³ /s, downstream water surface elevation (DWSE) = 869.9 ft.	31
Figure 25b. Barbs present, no sand bar present, discharge (Q) = 11,000 ft ³ /s, downstream water surface elevation (DWSE) = 869.9 ft.	31
Figure 26a. No barbs present, no sand bar present, discharge (Q) = 11,000 ft ³ /s, downstream water surface elevation (DWSE) = 869.9 ft.	32
Figure 26b. Barbs present, no sand bar present, discharge (Q) = 11,000 ft ³ /s, downstream water surface elevation (DWSE) = 869.9 ft.	32
Figure 27a. No barbs present, no sand bar present, discharge (Q) = 11,000 ft ³ /s, downstream water surface elevation (DWSE) = 869.9 ft.	33
Figure 27b. Barbs present, no sand bar present, discharge (Q) = 11,000 ft ³ /s, downstream water surface elevation (DWSE) = 869.9 ft.	33
Figure A1. External calibration, discharge (Q) = 315 ft ³ /s, downstream water surface elevation (DWSE) = 861.38 ft.	38
Figure A2. External calibration, discharge (Q) = 315 ft ³ /s, downstream water surface elevation (DWSE) = 861.38 ft.	38
Figure A3. External calibration, discharge (Q) = 315 ft ³ /s, downstream water surface elevation (DWSE) = 861.38 ft.	39
Figure A4. External calibration, discharge (Q) = 315 ft ³ /s, downstream water surface elevation (DWSE) = 861.38 ft.	39
Figure A5. External calibration, discharge (Q) = 250 ft ³ /s, downstream water surface elevation (DWSE) = 861.15 ft.	40
Figure A6. External calibration, discharge (Q) = 250 ft ³ /s, downstream water surface elevation (DWSE) = 861.15 ft.	40
Figure A7. External calibration, discharge (Q) = 250 ft ³ /s, downstream water surface elevation (DWSE) = 861.15 ft.	41
Figure A8. External calibration, discharge (Q) = 250 ft ³ /s, downstream water surface elevation (DWSE) = 861.15 ft.	41

1. INTRODUCTION

The North abutment of the U.S. Highway 169 Bridge, located on the Raccoon River central Iowa, is threatened by excessive bank erosion due to the formation and movement of a meander bend located upstream of the bridge. The meander bend (Figure 1) once located approximately 1800 ft upstream of the North bridge abutment has translated downstream to within 450 ft of the bridge. The observed bank erosion appears to be accelerating as the bridge acts as a control structure not allowing the downstream portion of the reach to adjust to changes upstream. The Iowa Department of Transportation (IDOT) decided that if allowed to continue unregulated, the bank erosion could be threatened to wash away the North bridge abutment thereby threatening the bridge's overall structural integrity. To mitigate this problem, the IDOT proposed two alternatives: 1) armoring the north bank of the Raccoon River with riprap from the bridge upstream approximately 1800 ft to increase the composite erosive strength of the bank, or 2) install a field of bendway weirs to increase the conveyance along the center of the stream to reduce the erosive force exerted on the bank by the river. The IDOT chose the second alternative based on the historical success of using bendway weirs for this application (Przedwojski et al., 1995).

Bendway weirs can effectively mitigate this process by redirecting the bulk streamflow away from the bank and into the center of the channel. An extensive literature review shows an abundance of data regarding flow locally around bendway weirs (e.g. Rajaratnam and Nwachukwu, 1983; Fox et al., 2005) and in the corresponding weir fields (e.g. Uijtewall, 2001; Sukhodolov et al., 2002). However, detailed design guidelines for bendway weirs to mitigate bank erosion are limited due to the site specificity involved (Przedwojski et al., 1995). Therefore, the design engineers are forced to rely on physical and/or computational models to predict the effects of bendway weirs into the riverine environment. Numerical models are often preferred over physical models due to the ease of simulating flows in multiple scenarios.

Recent advancements in numerical modeling have made computer models an increasingly attractive engineering tool for predicting changes in fluvial environments. Numerous commercially available hydrodynamic and sediment transport models now exist for various intended applications. These models differ in their spatial and temporal continua as well in their basic equations and underlying assumptions. Therefore, proper model choice is necessary to ensure the success of the design. Investigation into the typical flow processes around bendway weirs show that the flow in this location is highly turbulent (Fox et al., 2005), although the key morphological changes are the result of large scale two-dimensional flow structure (Melville and Coleman, 2000; Sukhodolov et al., 2002). The proper choice for a numerical model should be able to adequately account for the added dissipation of the turbulent flow while accurately reproducing the large scale flow effects around the structures in a channel replicating the actual study site.

Based on its proven track record (e.g. Kahn and Barkdoll, 2001; Matin and Elbert, 2004; Hobbs, 2005), the two-dimension depth averaged hydrodynamic Finite Element Surface Water Modeling System (FESWMS) was chosen for this study. Hobbs (2005) performed a detailed sensitivity analysis of FESWMS and utilized a calibrated model to evaluate the effectiveness of unsubmerged boulders as sediment traps in a steep-sloped river. Matin and Elbert (2004) successfully applied FESWMS for studying bank erosion calibrating his model for uniform flow within a straight section of the reach. Kahn and Barkdoll (2001) performed a study showing that

FESWMS is capable of accurately simulating flow around sharp river bends where secondary currents are prevalent.

The main objective of this study is to evaluate the hydraulic performance of riprap spurs and weirs in controlling bank erosion at the Southern part of the Raccoon River upstream U.S. Highway 169 Bridge utilizing the commercially available model FESWMS. The limitations and capabilities of FESWMS was first evaluated through a detailed sensitivity analysis of the input parameters in a reach containing bendway weirs second, the model were calibrated and verified using field measurements data. State of the art equipment and techniques were used to collect and analyze the field measurements data. Finally, in-bank and over-bank flow conditions were simulated using calibrated input parameters.

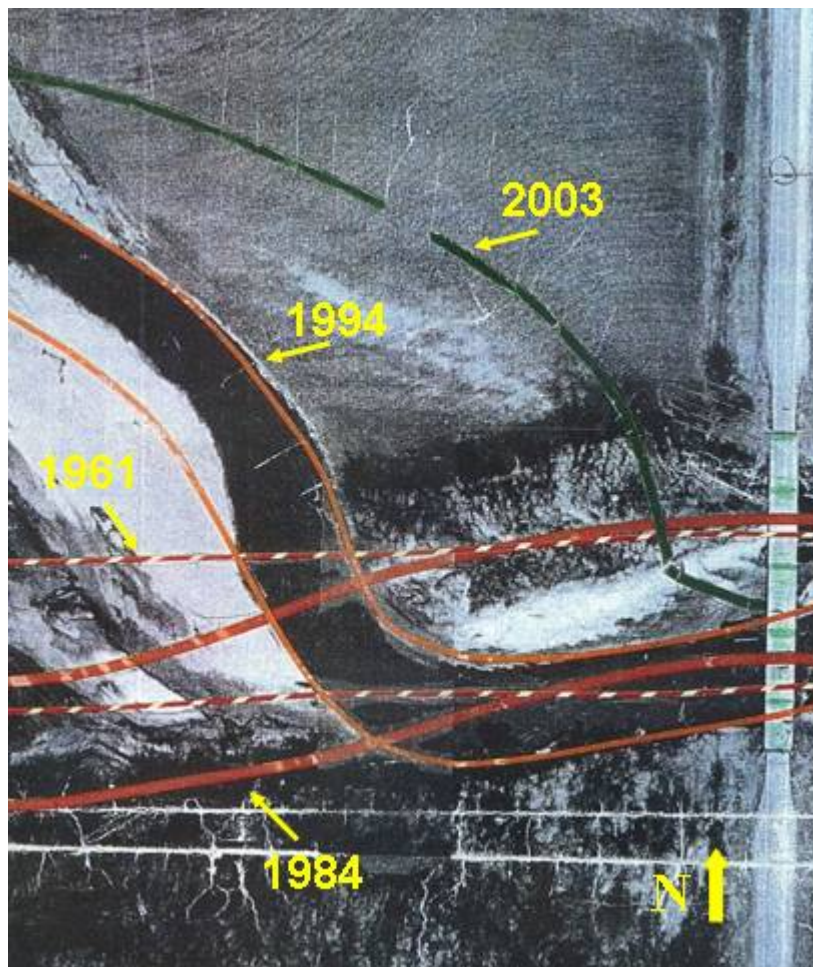


Figure 1. Observed movement of Raccoon River Channel Upstream of the U.S. Highway 169 Bridge (Claman, 2005). The various color bands represent the observed location of the streambanks during the year indicated. U.S. Highway 169 can be seen running North and South along the right hand side of the photo. Flow is from left to right.

2. STUDY SITE

The Raccoon River near Adel, Iowa, USA, is a mild gradient, unregulated, meandering river with medium to fine sand bed overlain with clay on the floodplain. The reach of interest has a bed slope of 0.00061 and an approximate sinuosity of 1.8 forming deeply entrenched corners with bank heights exceeding 10 ft. The sand bed has a d_{50} of 3.28 (10-3) ft and a coefficient of uniformity of 5.0. At the study site located just upstream of the U.S. Highway 169 Bridge towards the west, the Raccoon River possesses a watershed of approximately 1,116 mi² of primarily rural agricultural land. The average daily flow rates at the site is 210 ft³/s with annually reoccurring events producing flows of 1900 ft³/s (IDOT) and fifty year reoccurrence events producing flows as high as 35,000 ft³/s.

The IDOT bendway weir design constructed at the site uses a total of 9 structures with an average spacing to length ratio of 2.0: 1.0, and a contraction to width ratio of 2.0: 3.0. These structures are composed of piled riprap extending perpendicularly from the bank line out into the river. Figure 2 shows a typical bendway weir as constructed at the Raccoon River Study Site. The crest of the weir nose is located 2.5 ft above the streambed, and rises with a 6: 1 slope until it meets bank height. Typical weir lengths in the IDOT design range from 45 ft to 90 ft. The side slopes of the barb descend from the 8 ft wide crest at a 2.0: 1.0 slope. Five of the structures also possess the a 55 ft long, 8 ft wide, 2.5 ft tall submerged barb extending off of the toe of the structure. The subsequent weirs alternate between possessions of the barbs. Figure 3 shows the constructed bendway weir design looking upstream from the U.S. Highway 169 Bridge.



Figure 2. Typical bendway weir design as constructed at the Raccoon River study site. Picture taken from the channel center looking perpendicular at bank with flow going from left to right. The bridge (not pictured) is located downstream of this structure.



Figure 3. Constructed bendway weirs looking upstream from the U.S. Highway 169 Bridge.

3. METHODOLOGY

The focus of the proposed methodology is to evaluate the effectiveness of two-dimensional depth-averaged hydrodynamic model with reasonably assumed input parameters for Manning's coefficient and eddy viscosity in simulating the flow pattern around bendway weirs. This research is based on the assumption that bendway weirs performance can be predicted based on averaged characteristics of the flow. To be considered an appropriate approximation, the model must be properly calibrated to ensure accuracy and compare favorably with field observations. Furthermore, a sensitivity analysis of the inputted parameters for bed friction and eddy viscosity must be performed to identify controlling parameters affecting model performance. The overarching objective of this study is to prove that a well calibrated model can provide accurate qualitative and quantitative properties of flow around bendway weirs. The following major steps were incorporated into the methodological design to achieve the study objectives:

1. Identify critical characteristics of successful bendway weir that must be evaluated during the design stages.
2. Identify the most suitable two-dimensional code that can facilitate large scale hydrodynamic analysis of the mean flow characteristics within mild gradient sand bed river reach and is capable of mapping spatially and time averaged flow structures around bendway weirs.
3. Determine sources of uncertainty in the model input and understand their potential effects in the model output.
4. Collect flow measurements around bendway weirs at the study site for multiple flow events for model calibration and verification purposes.

5. Calibrate the model and verify the simulation accuracy through comparisons with select field measurements.

These major steps will be further discussed and analyzed with the methodological strategy of this investigation.

3.1 Critical Design Characteristics

Bendway weirs induce flow redistribution by redirecting the main bulk flow away from the bank towards the centerline of the channel. Fox et al. (2005) identified three distinct flow regions near a partly submerged weir as illustrated in Figure 4. These regions are the (1) main-core flow which extends from the tip of the weir to the main channel flow, (2) wake region consisting of pseudo-stagnant flow extending downstream of the structure, and (3) the shear-layer region which is formed between the fast moving main-core flow and the wake region. An accelerating zone is sought to occur in the vicinity of the shear layer boundary attributed to the low relative submergence (i.e., the ratio of the flow depth to the structure height) of the structure. The hydrodynamics of each of these regions is intimately involved in the performance of the structure.

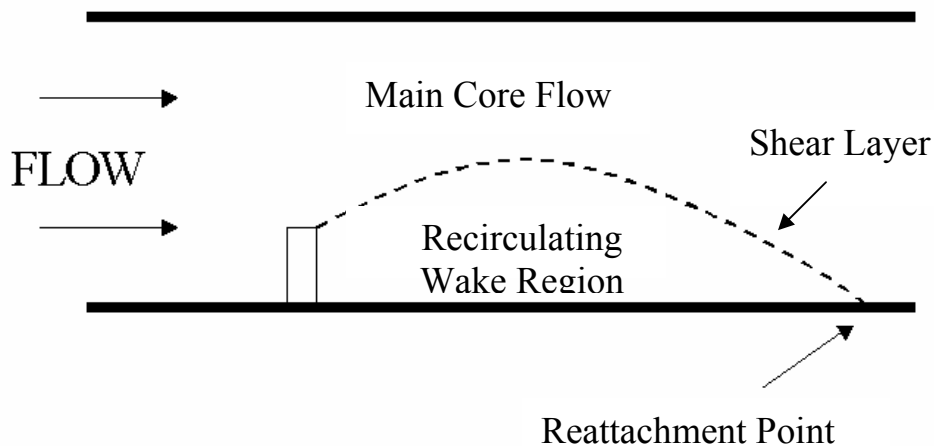


Figure 4. Typical flow structure near a bendway weir (plan view).

The flow acceleration couples with the structure induced turbulence to increase the magnitude of the flow induced bed-shear stress. This increase in stress allows for the entrainment of bed particles thereby producing scour. Although this scour may be attributed to both local and contraction effects, local and contraction scour are not distinguished (Melville and Coleman, 2000). These scour-holes have been found to have beneficial effects on local flora and fauna (Shields et al., 1998), but may also be detrimental to the stability of the structures (Przedwojski et al., 1995). Therefore, predicting the potential dimensions of these scour holes is a critical design step (Melville and Coleman, 2000). Accurately reproducing the spatially averaged flow properties in the main-core flow is necessary to provide localized flow velocity and depths for predicting the scour-hole geometry via empirical formulas. Ghodsian and Tehrani

(2001) determined the maximum scour depth for a spur dike to be a function of the following parameters for clear water scour:

$$ds = f1(\underbrace{V, y}_{\text{submergence}}, \underbrace{\rho_s, g, d_{50}}_{\text{particle velocity}}, \underbrace{B, L}_{\text{contraction}}, \underbrace{\theta}_{\text{angle}}, \underbrace{R}_{\text{permeability}}) \quad (1)$$

where V is the approach velocity of flow; y is approach depth of flow; ρ_s is density of sediment; ρ = density of water; g is acceleration due to gravity; d_{50} is mean sediment grain size; B is the width of main channel; θ is the angle of inclination, and R is the ratio of length of permeable part to impermeable part of structure.

The slow moving velocities of the wake region reduce sediment entrainment leading to the deposition of the sediment load. Understanding these depositional patterns can allow for the prediction of morphological changes that may occur in the reach. Sukhodolov et al. (2002) related the two-dimensional time averaged flow patterns of the wake region to corresponding depositional patterns and morphological changes. Chen and Ikeda (1997) also provide relationships between the mass and momentum exchange occurring laterally through the shear layer as a function of the time-averaged streamwise velocity, transverse velocity, and flow depth. This knowledge can be useful to designers for ensuring enough mass exchange occurs to maintain an inhabitable environment in the wake region.

The spatial dimensions and flow attributes of the stagnant wake region found downstream of the structure are also necessary in predicting the performance of the design. In an isolated condition where local flow characteristics are not affected by any downstream structures, the wake region consists of recirculating flow with a streamwise length extending from the structure downstream to the point where the main stream flow reattaches to the bank. This length is defined as the reattachment length (Schmidt et al., 1993). The reattached flow typically produces undesired bank erosion at the reattachment point due to the increase of shear stress caused by the flow impinging on the bank. This makes it imperative from a design standpoint that the main stream flow is not allowed to reattach to the bank throughout the project area.

The reattachment length is directly proportional to the length of the bendway weir (Ettema and Muste, 2004), therefore, the spacing between structures is dependant upon the structure length and typical design specifications also include spacing to length ratio (S/L). Przedwojski et al. (1995) provides results from numerous studies with recommended S/L ratios and Sukhodolov et al. (2002) provides empirical data of expected flow patterns for different S/L ratios (Figure 5). Ettema and Muste (2004) outlined the important parameters defining thalweg depth, alignment, sinuosity, and separation region around a single structure. These parameters are:

$$f(T_D, T_C, L, W, T_U, B_1, B_2) \quad (2)$$

where T_D is the downstream distance required for the thalweg to realign with the channel, T_C is the maximum lateral location of the thalweg in the short subreach, L is the length of the structure, W is the unobstructed width of the channel, T_U is the distance upstream of the structure at which thalweg shifts from the channel centerline, and B_1 and B_2 are respectively the maximum downstream extent and lateral width of the flow separation region.

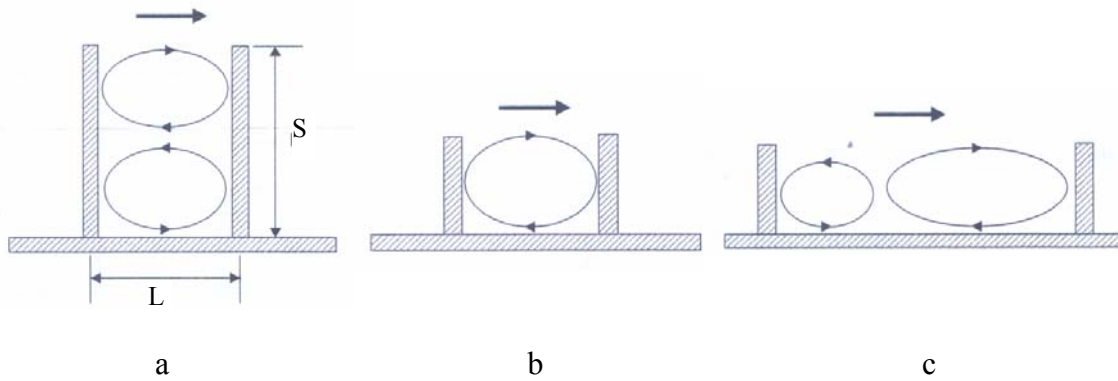


Figure 5. Typical flow patterns in a groyne field (plan view): a) $S/L < 0.5$; b) $0.5 < S/L < 2.0$; and c) $S/L > 2.0$.

The maximum length of the structure is inherently limited by the width of the river, although the actual length of the structure is primarily a function of how much the designer desires to redirect the flow (Przedwojski et al., 1995). Typical design specifications will include a length to stream width ratio (L/B). It is obvious that as this ratio approaches the value of 1, the flow will become increasingly contracted escalating the amount of contraction scour that will take place and possibly causing flow impingement on the far river bank. Maximum recommended L/B values are approximately 0.5 (Przedwojski et al., 1995).

Introducing structures to the channel have large scale effects on the river. Structures increase the total flow resistance of the channel and can create backwater effects during high flow events. Adjusting the streamlines in an upstream portion of the reach may also produce unwanted effects downstream. It is therefore in the engineer's best interest to model the entire series of structures in natural geometry representative of the study reach and extending both upstream and downstream of the project site to fully understand these large scale effects.

Bendway weir designs have been extensively studied in recent years. Although no definitive design specifications exist, there are many broad design guidelines. Bendway structures are typically composed of stone, gravel, rock, earth, or pile and are built either perpendicular to or at an angle to the upstream river bank. They geometries typically have a higher crest elevation near the bank and slope downward toward the center of the river. This crest pairs with a trapezoidal cross-sectional shape reduce the velocity gradient as the submerged shape broadens the mixing layer between the main stream and groyne field (Uijttewall, 2005).

3.2 Choice of Numerical Model

Two-dimensional models can adequately resolve large scale flow patterns and provide shear stress distributions necessary for sediment transport calculations over complex bathymetric geometry (Kahn and Barkdoll, 2001). Based on these attributes and the limited amount of calibration data required, a two-dimensional model was determined to be the optimal tool for bendway weir design within a reach scale. Selection of the proper two-dimensional model was based on a set of five desired capabilities as outlined by Hobbs (2005). These capabilities are:

1. The model should be able to handle all the relevant processes of flow around hydraulic structures including but not limited to the advective and diffusive nature of flow within the water column, transcritical flows, and abrupt variations in velocity.

2. The model should be able to provide the bed shear stresses for sediment transport applications.
3. The model should allow for multiple material properties to be present in a reach and for these material properties to be easily varied providing better calibration potential.
4. The model should have a known track record of being applied successfully to similar applications to best understand its capabilities and limitations.
5. The model should allow easy grid modification over natural bathymetric geometry.

Based on the above criteria, the Surfacewater Modeling System (SMS) version 9.0 graphical interface and the Finite Element Surface Water Modeling System (FESWMS) were chosen for this study. SMS is a package of software which includes a number of two-dimensional hydrodynamic and sediment transport models as well as pre- and post-processing tools. It has a user-friendly graphical interface and is capable of generating two-dimensional grids over variable realistic bathymetric geometry. SMS allows for the elements of the computational grid to easily be assigned individual material properties. Furthermore, FESWMS has provided satisfactory results in similar applications such as Hobbs (2005) who showed the model could accurately reproduce the large scale effects of introducing large scale structures into a steep river reach, Khan and Barkdoll (2001) who showed FESWMS could accurately reproduce velocity magnitudes in river bends where secondary currents are prevalent, and Matin and Elbert (2004) who used FESWMS in a bank erosion case study.

FESWMS was developed for the Federal Highway Administration to model flow around bridge piers (Froelich, 2002). The model includes provisions for modeling structures such as weirs and inlets, and is capable of modeling flows with hydrostatic pressure. FESWMS, a finite element code, utilizes the Galerkin method of weighted residuals to solve differential forms of the continuity and momentum equations in both the streamwise and transverse directions to provide a velocity vector and flow depth at each node in the computational grid (Froelich, 2002). The conservative form of the equations allows for momentum to be conserved along a streamline and can therefore capture shock such as in transcritical flows (Chaudhry, 1993). Equations written in conservative form are also capable of simulating flows in complex cross-sectional geometries under both low and high flow conditions by allowing “dry” elements to exist within the stream reach.

The differential form of the continuity equation in FESWMS is given as

$$\frac{\partial Z_w}{\partial t} + \frac{\partial q_1}{\partial x} + \frac{\partial q_2}{\partial y} = q_m \quad (3)$$

where Z_w is the elevation of the water surface in the vertical direction above a datum, q_1 and q_2 are mass fluxes defined as the product of the streamwise depth averaged velocity, \bar{u} , and depth of the water column, d , and transverse velocity, \bar{v} , and column depth, d , respectively, and q_m is the resultant mass inflow or outflow flux. The momentum equations are given as

$$\begin{aligned} \frac{\partial q_1}{\partial t} + \frac{\partial}{\partial x} \left(\frac{q_1^2}{d} + \frac{1}{2} g d^2 \right) + \frac{\partial}{\partial y} \left(\frac{q_1 q_2}{d} \right) + g d \frac{\partial Z_b}{\partial x} - \frac{1}{\rho} \lambda \rho_a V_a^2 \cos \psi \\ + g n^2 \frac{q_1 \sqrt{q_1^2 + q_2^2}}{d^{7/3}} \sqrt{1 + \left(\frac{\partial Z_b}{\partial x} \right)^2 + \left(\frac{\partial Z_b}{\partial y} \right)^2} - 2d \varepsilon_{xx} \frac{\partial^2 \bar{u}}{\partial x^2} - \varepsilon_{xy} \frac{\partial}{\partial y} \left(\frac{\partial \bar{u}}{\partial x} + \frac{\partial \bar{v}}{\partial y} \right) = 0 \end{aligned} \quad (4)$$

$$\begin{aligned}
& \frac{\partial q_2}{\partial t} + \frac{\partial}{\partial x} \left(\frac{q_1 q_2}{d} \right) + \frac{\partial}{\partial y} \left(\frac{q_1^2}{d} + \frac{1}{2} g d \right) + g d \frac{\partial Z_b}{\partial y} - \frac{1}{\rho} \lambda \rho_a V_a^2 \sin \psi \\
& + g n^2 \frac{q_2 \sqrt{q_1^2 + q_2^2}}{d^{7/3}} \sqrt{1 + \left(\frac{\partial Z_b}{\partial x} \right)^2 + \left(\frac{\partial Z_b}{\partial y} \right)^2} - \varepsilon_{yx} \frac{\partial}{\partial x} \left(\frac{\partial \bar{u}}{\partial x} + \frac{\partial \bar{v}}{\partial y} \right) - 2 d \varepsilon_{yy} \frac{\partial^2 \bar{v}}{\partial y^2} = 0
\end{aligned} \tag{5}$$

where x is the streamwise direction, y is the transverse direction, g is the gravitational constant, Z_b , is the elevation of the bed above a datum, ρ is the density of water, λ is a wind constant, ρ_a is the density of air, V_a , is the wind velocity, ψ is the wind direction, and n is the Manning's coefficient. ε_{xx} , ε_{xy} , ε_{yx} and ε_{yy} denote the eddy viscosity in the streamwise direction, the streamwise direction with respect to the transverse direction, the transverse direction with respect to the streamwise direction, and the transverse direction, respectively.

3.3 Sources of Model Uncertainty

The output of each FESWMS simulation is dependant upon user input values for Manning's coefficient, eddy viscosity, and the momentum correction coefficient for the velocity distribution (Hobbs, 2005). Hobbs (2005) showed varying the momentum correction coefficient had trivial affects on the model output, therefore only the Manning's coefficient and eddy viscosity input parameters were analyzed in this study. To produce accurate results, these input values must correctly represent the actual physical processes occurring in the modeled reach. Unfortunately, both of these inputs are empirically derived values. Although these parameters have been well documented in the literature (e.g. Miller and Cluer, 1998), they are typically provided as a range of values and are difficult to apply to other studies because of their strong dependence on specific site conditions. It is therefore necessary to calibrate the model using input values which reflect actual conditions found in the study reach to ensure model accuracy. For this particular study which examines the models intended capabilities, it is essential to determine that the model is not overly sensitive to variations in the input values. These input values are subject to both spatial and temporal variation almost ensuring some form of input error. All of the causes of the input variability must be identified so their effects can be fully understood.

The Manning's coefficient value is an empirical value that accounts for the total flow resistance caused by flow interaction with the boundary (Hicks and Mason, 1991). Traditionally, a constant Manning's coefficient value is applied throughout a reach to represent the spatially averaged roughness for one-dimensional flow and implicitly accounts for effects of turbulence and horizontal variation in velocity (Froelich, 2002). FESWMS utilizes Manning's coefficient solely to account for momentum loss due to bed shear which may randomly vary throughout a channel in accordance with micro-structures (i.e. bed forms too small to be incorporated into the bathymetric data of the mesh). It is also difficult to separate the combined effect of form and skin roughness when spatially discretizing Manning's coefficient. Although FESWMS possesses the capability to spatially distribute Manning's coefficient, it is not feasible to reproduce its random spatial distribution in the model. The inconsistency between the use of Manning's coefficient in one-dimensional and two-dimensional modeling, the inability to reproduce its spatial distribution, as well as the difficulties in predicting its actual value, generates a reasonable amount of uncertainty that must be associated with an estimated Manning's coefficient input. It

is therefore reasonable to assume that some error will be incorporated into the model due to the inability to exactly match roughness values at all locations in a modeled reach.

The other flow resistance term used by FESWMS is eddy viscosity. The eddy viscosity value accounts for the added energy dissipation due to turbulence in the flow (Bridge, 2004). Whereas Manning's coefficient accounts for flow resistance due to shear stresses between the fluid and the boundary, eddy viscosity accounts for flow resistance due to the internal shear stresses, or Reynolds' stresses, of the fluid. Therefore, eddy viscosity is a property of the flow condition and not of the fluid itself. This produces a conundrum in that the flow simulation is dependant upon the inputted eddy viscosity value which in turn is dependant upon the unknown flow properties sought in the simulation. Fortunately, eddy viscosity values for uniform flows can be assumed as a function of depth and bed slope. In this study application, however, it is expected that the flow near the structure would be highly turbulent and the local eddy viscosity would therefore be much higher than for the flow located away from the structure. It is likely that assumed input values of eddy viscosity will possess some error or lack adequate spatial resolution. To fully endorse FESWMS as a viable tool for designing bendway weirs to mitigate bank erosion, it must be shown that any slight variations in the eddy viscosity values are not amplified in the simulation results.

Another parameter that must be evaluated is the Peclet number. The Peclet number is the ratio of advection to dispersion occurring in an element and is defined as

$$Pe = \frac{\bar{u}\Delta x}{\sqrt{\varepsilon_{xx}^2 + \varepsilon_{yy}^2}} \quad (6)$$

It is recommended that the Pe be kept between 10 and 30 to accurately resolve flow patterns (Miller and Cluer, 1998; Froelich, 2002). Satisfying the Peclet criteria ensures that proper amount of energy loss due to dispersion takes place in each element to account for micro-eddies which are too small to be resolved in the mesh (i.e. those eddies that are smaller than the local element size). Inspection of the Peclet equation shows that the mean streamwise velocity and eddy viscosity determine the ideal grid spacing, Δx , and therefore the minimum eddy length that can be resolved. However, the grid spacing is also function of the local geometry, including bed roughness, and tailoring a grid design to ensure a constant Peclet number throughout the reach is laborious and unreasonable. It is therefore essential to show that small variation in the Peclet number throughout the reach will not results in significant error.

Because the above input parameters in FESWMS possess uncertainty, it is important to evaluate the model's sensitivity to each variable. If a model is overly sensitive to a particular input value, the uncertainty of the input value becomes amplified in the results. An important step in identifying a model's limitations is to determine these sensitivities and their potential effects. Quantifying the output uncertainty as a function of the total input uncertainty through a sensitivity analysis offers a better understanding of a model's precision.

3.4 Data Collection for Model Calibration

Although the sensitivity analysis can locate and quantify sources of error due to variability in parameter values, it cannot verify a model's accuracy. The model's accuracy must instead be evaluated through the comparison of results from a properly calibrated simulation to field measurements from a physical reach with identical flow conditions. While input parameters can

be reasonably approximated (e.g. using readily available discharge data), it is within the scope of this study to also measure and verify the inputted parameters to fully understand the models capabilities in accurately reproducing the flow patterns around bendway weirs. Field measurements were performed in the study reach of the Raccoon River near the constructed bendway weirs. These measurements included detailed, non-intrusive point velocity measurements with the use of a SonTek Acoustic Doppler Velocimeter (ADV), aerial velocity measurements through the use of large scale particle image velocimetry (LSPIV) technology, and bathymetric measurements using a combination of an Eagle FishElite® 480 sonar and standard surveying practices.

The ADV uses Doppler technology to calculate instantaneous point velocity measurements in a 0.25 cm³ sampling volume. Typical ADV sampling rates of 25 Hz allow for the turbulent velocity fluctuations to be adequately captured for evaluation of Reynolds' stresses. The velocity profile can also be determined from time averaged velocity results over a range of depths at a single point (Papanicolaou and Hilledale, 2002). Coupling this data yields the kinematic eddy viscosity by definition of

$$\varepsilon = \frac{\overline{u'v'}}{\partial \bar{u} / \partial y} \quad (7)$$

which is then used to verify the eddy viscosity values inputted into the model. Determining the velocity profile can also verify the built-in FESWMS assumption of a logarithmic velocity profile. Furthermore, the subsequent calculation of the shear velocity when finding the velocity profile can be used to verify bed shear values calculated in the model.

LSPIV technology is an image-based approach for measuring time averaged surface velocities over large areas (>2500 ft²) (Creutin et al., 2003). This non-intrusive method, which is based on the more common particle tracking velocimetry (PTV) used in controlled laboratories, can provide large data sets of simultaneously measured velocity vectors and resolve large scale flow patterns. Both of these results are advantageous for verifying the use of a two-dimensional depth averaged model. Unlike three-dimensional models which require knowledge of the small scale instantaneous velocity for different turbulent closure schemes near the boundary, the time averaged depth averaged two-dimensional models can only be verified based on depth and time averaged velocities. Therefore the large sample size provided by the LSPIV allows for better statistical comparison of measured to calculated velocity values. Furthermore, it is vital in this study to show that the model not only match velocity and depth magnitudes, but the overall flow pattern as well.

Bathymetric measurements were required to gain depth measurements for model calibration and to verify the quality of the bathymetric data provided by the IDOT. The Eagle Fish Elite 480 is a coupled sonar/GPS instrument capable of recording both depth and corresponding positional data at a rate of 1.0 Hz. This allowed for large sample of depth measurements to be recorded for use in the model calibration process. Because the Fish Elite 480 is not capable of recording elevation, standard surveying practices using a Topcon GTS 226 total station were used to measure the water surface elevation. The total station was also used to collect depth measurements for verifying the sonar data, as well as the dimensions of the constructed structures. Appendix 1 of this thesis provides methodology for recording depth measurements and algorithm for converting the data to desired units.

Field measurements were conducted under two separate low flow conditions. It is during these low flow conditions that the structures have the largest impact on the flow pattern and parameters such as eddy viscosity and bed shear vary the greatest throughout the reach (Papanicolaou and Hilldale, 2002). It is also during these low flows that the input parameters will have the greatest influence on the model results; thereby testing the model in the most extreme conditions. Although the structures were in existence for less than one year prior to measurement, several high flow events with return periods of one year occurred prior to the measurements and the overall bed average features were assumed to be in a quasi-equilibrium state. This ensured that no significant changes would occur throughout the entire flow event. The latter assumption facilitated the use of FESWMS with immobile bed geometry.

3.5 Model Calibration

To fully endorse FESWMS as being a reliable tool in the design of bendway weirs to mitigate bank erosion, it must be proven that the model can accurately resolve the proper flow patterns, velocity magnitudes, and depths as measured in the field. The model should be able to provide accurate results with reasonably accurate input parameters which reflect the actual physical processes occurring in the reach. If these input parameters require large adjustments for the simulation to match the values, then the adjustments must be quantifiable and physically justifiable.

Model simulations were run using bathymetric data collected during an IDOT survey in July 2005 and appended with field data. Design geometries for the bendway weirs were incorporated into the model and verified with a field survey after construction. The SMS projects inputted bathymetric data onto the computational grid using an inverse-distance weighted algorithm to assign node elevations based on the elevations of the nearest 16 bathymetric points. Excavation of a new channel just upstream from the U.S. Highway 169 Bridge rerouted daily flows away from the downstream structures prohibiting their use in the calibration study. Flow around the four furthest upstream structures was assumed unaffected by this channel relocation. The flow pattern around these structures is consistent with those recorded in literature prompting the study area to center on these structures.

The computational mesh used in the calibration process is shown in Figure 6. This mesh, composed of both six-node triangular and eight-node quadrilateral elements, was created in SMS using both the paving and patch techniques. The paving technique produces an unstructured grid of triangular elements and was used along both bank lines and near the structures to provide better spatial resolution of the irregular geometry. The patch technique produces a structured grid of quadrilateral elements and was used along the relatively uniform bathymetric center of the channel to help reduce computational time. Bathymetric variation in quadrilateral elements can be lost due to the averaging of the larger elemental area that occurs with the integration used in the finite element process. However, the use of quadrilateral elements rather than triangular elements greatly reduces the computational expense of the mesh by reducing the front bandwidth of the global finite element matrix. Grid spacing was based on ensuring both the geometric variation of the reach was adequately captured and that the Peclet criterion was satisfied. For two-dimensional models, spatial resolution of the geometry has been found to have a greater effect than other input parameters in altering the hydraulic simulations (Hardy et al., 1999). Values for evaluating the Peclet number were based on velocity values measured in the field measurements and a constant depth-averaged eddy viscosity measured at the channel centerline.

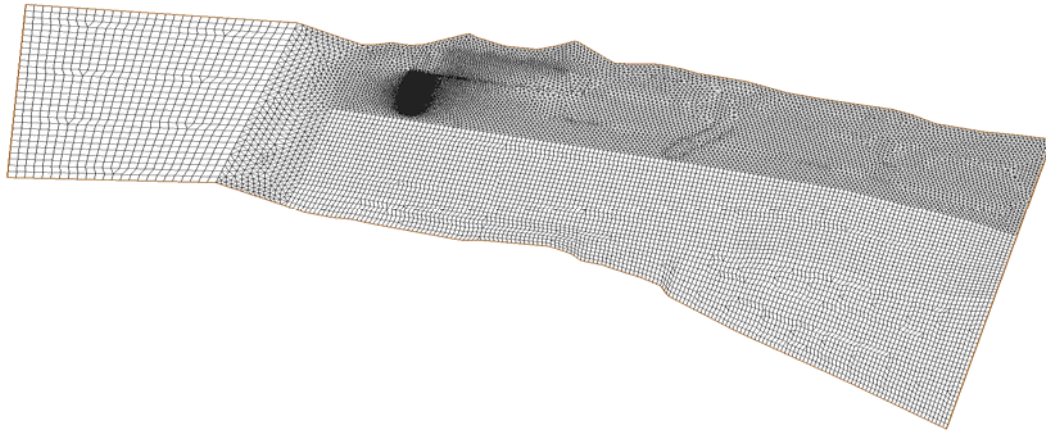


Figure 6. Computational Mesh used for model calibration. Flow is from left to right.

Simulations with boundary conditions corresponding to the flow events of the field measurements were run and compared to field measurements. Measured values for eddy viscosity, and bed shear were used to initially calibrate the input parameters. The model was first evaluated on its ability to quantitatively match the velocity magnitudes and flow depths in a large cross-sectional area. This initial “external” calibration ensures an accurate reproduction of the average flow patterns that are occurring throughout the reach. Once these values were reasonably matched, a more refined “internal” calibration process was focused in the area of interest near the structure. Flow patterns in this area were further scrutinized and more detailed material properties were inputted to increase the quality of the local results. The presence of the structure produces high spatial variability of material properties in this area as the turbulent properties of the flow causes the velocity profile to violate its assumed logarithmic shape and minimizes the effects of momentum loss due to bed shear.

The calibration process was based on the comparison of measured depth and velocity magnitudes to the calculated depth and resultant velocity magnitudes. The agreement between these values was analyzed by plotting the measured values vs. their respective calculated values. A line of perfect agreement passing through the origin and having a slope of one was plotted to allow comparison to the ideal situation. Understanding that variability will exist due to uncertainty in both the measured and calculated values and that some error was acceptable, two lines representing positive and negative 25 percent error relative to measured values were also drawn. The relative error was calculated as

$$E = \frac{V_{meas} - V_{Calc}}{V_{meas}} \quad (6)$$

where E is the relative error, V_{meas} is the measured value, and V_{Calc} is the calculated value. The “internal” calibration was also evaluated by comparing measured resultant velocity magnitudes to calculated resultant velocity magnitude along 20 transects. This point by point comparison provided more insight into the model’s capability to match the flow patterns. All results were further evaluated based on a qualitative comparison of vector fields produced from the measured and calculated data.

4. MODEL BEHAVIOR AND CALIBRATION

4.1 Sensitivity Analysis

Sensitivity analysis was performed for the main control parameters inputs, namely: the Manning's coefficient and the eddy viscosity. The behavior of the model was tested for different values of these two parameters. The sensitivity analysis of FESWMS was conducted over a straight reach having a length of 300 ft and width of 50 ft (Figure 7). The bed slope was mild and equal to 0.00061. Two bendway weirs are placed along the left bank of the channel. The distance of the first weir from the channel entrance is 50 ft. The same distance separates the downstream weir from the upstream weir. The weirs extend perpendicularly out from the bank 25 ft with a slope of 2.0: 1.0.

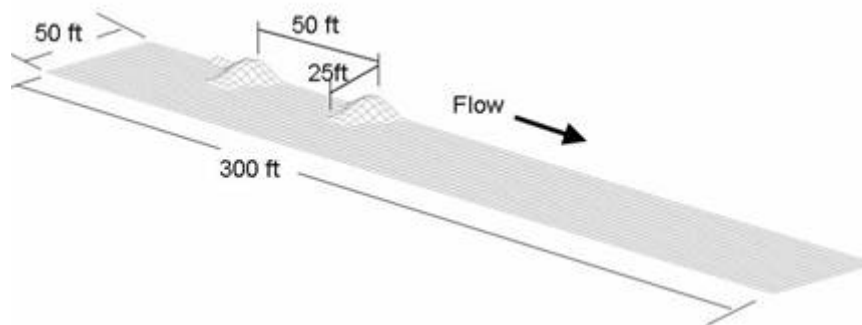


Figure 7. Simplified channel used in sensitivity analysis.

Two main scenarios have been considered for three flow events. The first scenario calls for a variable Manning's coefficient and fixed eddy viscosity of $0.42 \text{ ft}^2/\text{s}$ (Table 1). The practical implication of this condition suggests that model calibration should be performed for low flow conditions since high flows tend to mask the impact of Manning's coefficient on the velocity sensitivity. The second scenario calls for a fixed Manning's coefficient of 0.03 and variable eddy viscosity (Table 1). It was observed that reducing the eddy viscosity magnitude lowering the resultant velocity magnitude atop the bendway weir structures. Tables 2 and 3 summarize the reattachment lengths for the two scenarios. For first scenario, it was found that during high flow events the reattachment length remains nearly constant showing that Manning's coefficient has little impact on the reattachment length. For the high flow condition, the ratio of the reattachment length to the unsubmerged length of weir was approximately 7, which agrees with reported values in literature (e.g., Alvarez, 1989; Lagasse et al., 1995). In the second scenario, as the flow increases the reattachment length reduces with an increase in eddy viscosity. This trend is expected since as viscosity increases, the flow dissipates and reattaches at close vicinity downstream of the structure (Mayerle et al., 1995).

Table 1: Summary of the flow conditions and sensitivity analysis parameters.

Flow Condition						First Scenario (fixed eddy viscosity of 0.42 ft ² /s)	Second Scenario (fixed Manning's coefficient of 0.3)
1		2		3			
Q ft/s ³	H ft	Q ft/s ³	H ft	Q ft/s ³	H ft	Manning's coefficient	Eddy viscosity ft ² /s
1140	9.5	420	3.5	120	3.5	0.015	0.20
						0.020	0.40
						0.025	0.60
						0.030	1.00
						0.035	10.00
						0.040	20.00
						0.045	

Table 2: Reattachment length for various Manning's coefficient values.

First Scenario (fixed eddy viscosity of 0.42 ft ² /s)	Flow Condition					
	1		2		3	
	Q ft/s ³	H ft	Q ft/s ³	H ft	Q ft/s ³	H ft
	1140	9.5	420	3.5	120	3.5
Manning's coefficient	Reattachment Length ft					
0.015	56		180		185	
0.020	56		135		93	
0.025	55		108		75	
0.030	53		90		90	
0.035	52		78		63	
0.040	51		70		51	
0.045	50		65		45	

Table 3: Reattachment length for various eddy viscosity values.

Second Scenario (fixed Manning's coefficient of 0.3)	Flow Condition					
	1		2		3	
	Q ft/s ³	H ft	Q ft/s ³	H ft	Q ft/s ³	H ft
	1140	9.5	420	3.5	120	3.5
Eddy viscosity	Reattachment Length ft					
0.20	65		95		95	
0.40	55		90		90	
0.60	50		80		85	
1.00	45		65		75	
10.00	20		30		35	
20.00	15		25		30	

4.2 Field Measurements for Model Calibration

The second stage of the study involves the acquisition of field measurements during two separate low flow conditions, $Q = 315 \text{ ft}^3/\text{s}$ and $Q = 250 \text{ ft}^3/\text{s}$, and the utilization of this data for the subsequent calibration of the model. For the $Q = 315 \text{ ft}^3/\text{s}$ flow event, cross-sectional velocity measurements and sonar bathymetric measurements were employed to calibrate FESWMS for the main core flow roughness characteristics. In other words, the goal of this first exercise was to determine the most suitable Manning's coefficient value that accurately represents the roughness height within the main flow region (Appendix 1). This exercise was thought to be important after the findings of the flow sensitivity analysis for the straight channel demonstrated that the model was extremely sensitive to the choice of the Manning's coefficient roughness for low flow conditions. It was also determined in the prior section that a low Manning's coefficient value could closely replicate the reattachment length.

Figure 8 illustrates the location of the cross-sectional measurements for the $Q = 315 \text{ ft}^3/\text{s}$ flow event. The cross-sectional velocity measurements were obtained by means of the LSPIV technique for the surface velocity vector. Figure 9 provides a plan view image of the velocity vector field imposed atop of the velocity contour map showing the absolute magnitude of the velocity. An interrogation area (IA) of 50×50 pixels was set for the determination of the velocity. 50 pixels in the x -direction corresponded to 14.76 ft whereas in the y -direction 50 pixels were equal to 24.6 ft. The particle tracking velocimetry (PTV) algorithm searched around the IA within an average area of $1.0 \text{ ft} \times 1.0 \text{ ft}$. An iterative process was used to filter the data for various minimum correlation coefficients. It was determined that the optimal minimum correlation of 0.30 would provide an ample sample size of velocity measurements while removing enough poor quality data (Cruetin et al., 2003). The data was further filtered to not include measurements which exceeded the maximum velocity magnitude in the x -direction of 1.97 ft/s, or that were below the minimum velocity magnitude in the x -direction of zero. Similarly, velocities which exceeded 0.49 ft/s or were below -0.49 ft/s were not included when time-averaging the velocity measurements.

The upper and lower velocity limits were determined after some preliminary analysis of the flow under normal flow conditions. The standard deviation of the spatially averaged velocity was determined to be 0.45 ft/s. To verify the accuracy of the LSPIV measurements, the velocity distribution along the transect was integrated over the depth by assuming a logarithmic velocity profile. The integration provided the estimated discharge to be equal to $347 \text{ ft}^3/\text{s}$. The comparison of the estimated discharge with the measured discharge value ($315 \text{ ft}^3/\text{s}$) from the nearest USGS gaging station on the Raccoon River near Redfield, IA shows a deviation of less than 10%, indicating that the LSPIV procedure was conducted properly.

As part of the model calibration process, the Manning's coefficient value was initially set equal to 0.035 to coincide with values typically used in similar sand bed Midwestern streams. The eddy viscosity was assumed to be well described by the depth-averaged parabolic profile and was estimated to be $0.06 \text{ ft}^2/\text{s}$. According to Hobbs (2005) and Mayerle et al. (1994), the depth-average parabolic profile is suitable for describing the eddy viscosity distribution within the main channel. The estimated values for Manning's coefficient and eddy viscosity were used as inputs to the $Q=315 \text{ ft}^3/\text{s}$ run.

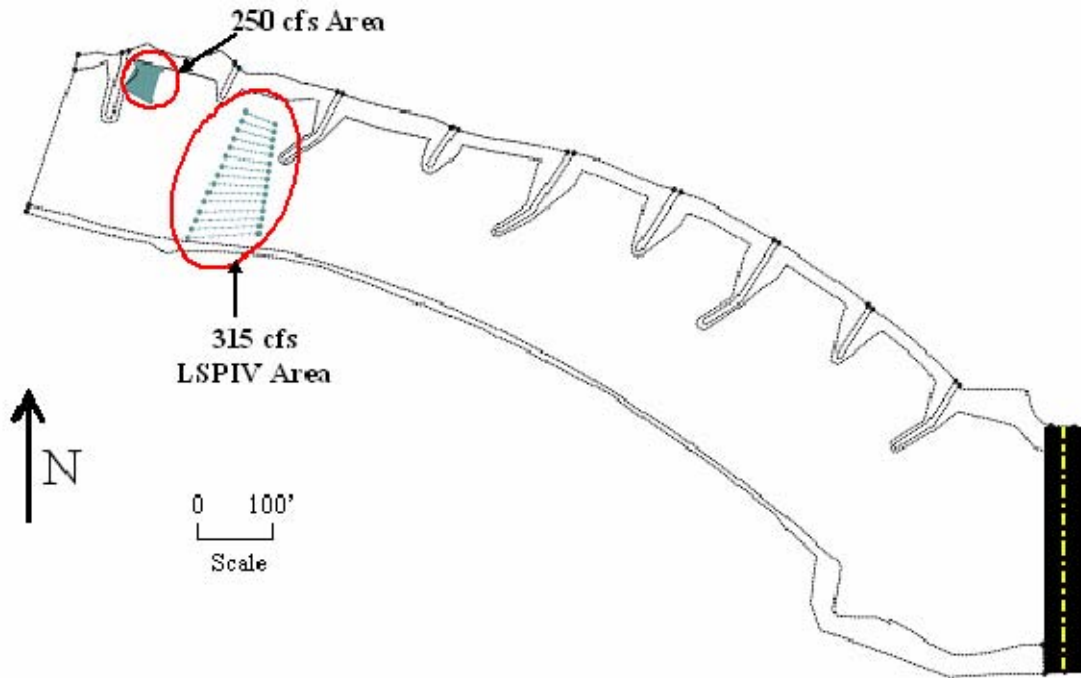


Figure 8. Locations of LSPIV Measurements.

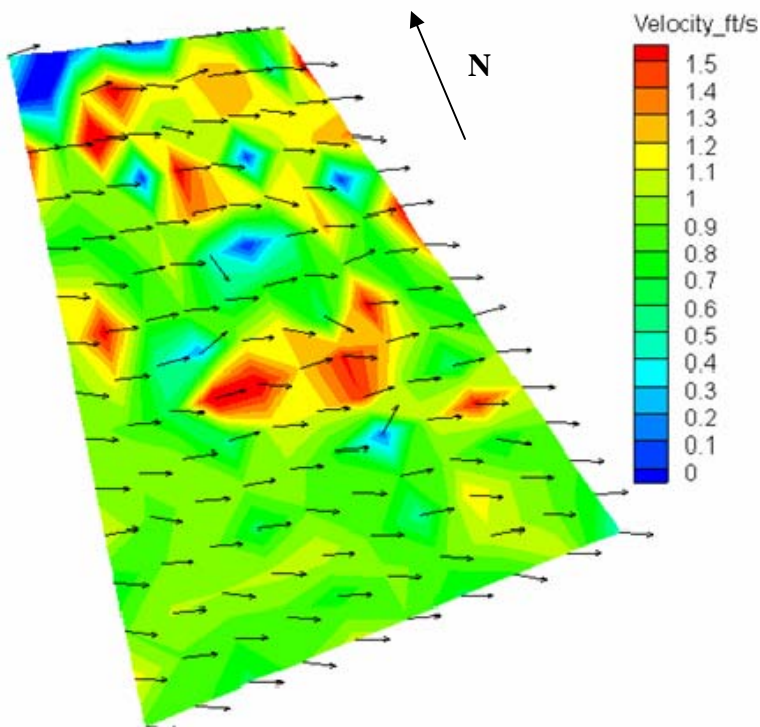


Figure 9. LSPIV velocity measurements for $Q=315 \text{ ft}^3/\text{s}$ flow event.

Once the model calibration for the main flow region was completed, it became apparent that the model ought to be calibrated for the internal region, defined herein as the localized area between two neighboring bendway weirs. For this purpose, LSPIV measurements were made in the wake region of the furthest upstream bendway weir. The LSPIV measurements revealed that a single cell recirculation pattern was formed between the adjacent weirs. The wake region behind the structure was apportioned into nineteen sub elements. Overall twenty transects were formed and the magnitude of the measured velocity along those transects was recorded (Figure 10). The measured velocity along these transects obtained a characteristic “V” shape distribution with the highest velocities being at the two ends, and the lower velocity roughly at the center of the transect. The “V” shape profile confirmed a recirculation pattern that was visually observed in the wake region of the bendway weir. The above method provided satisfactory results and allowed a closed depiction of the flow patterns in the vicinity of the structure by FESWMS.

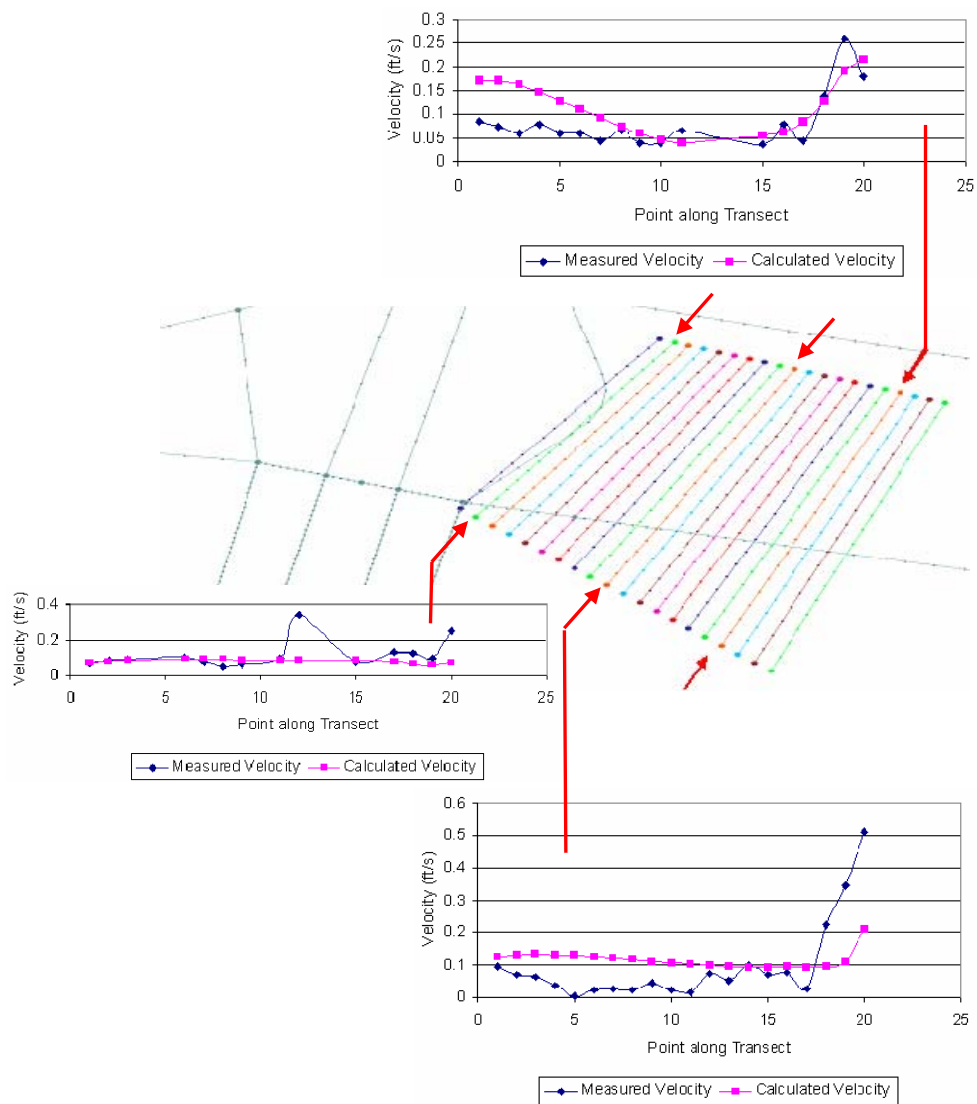


Figure 10. Comparison of measured and calculated values for selected transects. (Point 0 of the transect is nearest to the bank and point 20 is closest to the channel centerline).

Figure 11 provides a detailed plan view of the ADV measuring locations around the furthest upstream partially submerged bendway weir. The main purpose of the ADV measurements was to map the eddy viscosity spatial distribution around the structure. This information was used for model calibration in the inner region. A second goal of the ADV measurements was to determine if the mean flow conditions were highly three-dimensional or if the flow had a two-dimensional nature (Figure 12).

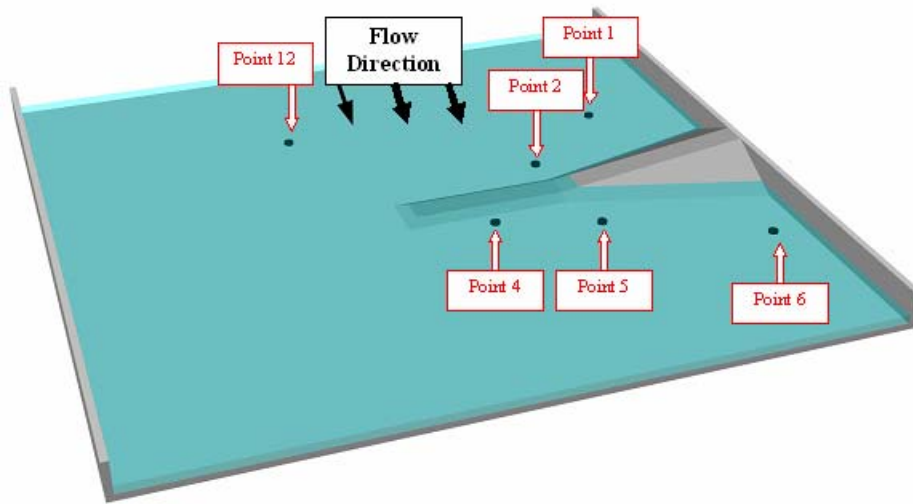


Figure 11. Location of ADV measurements relative to the bendway weir.

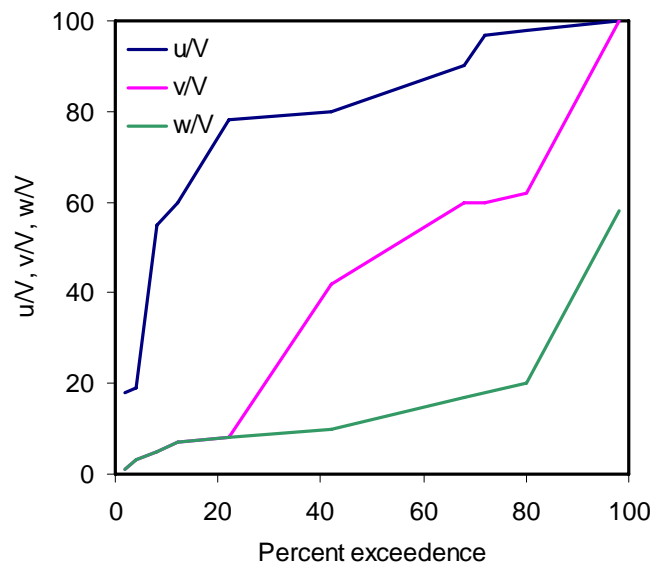


Figure 12. Analysis of the measured ADV velocity components.

4.3 Error Analysis

Evaluation of the ability of FESWMS to predict flow within the Raccoon River site was tested by comparing first the flow depth generated by the model against the depth measured in the field via the sonar. The Manning's coefficient value was adjusted iteratively until these depth measurements agreed and the velocity flow field best represented the observed flow conditions. Figure 13 demonstrates the effectiveness of the model in predicting the measured flow depth. It is shown that the simulated flow depth along the transect is always within 25% of the measured flow depth. Although the acceptance criteria for depth and flow modeling are still very much subjective and may vary significantly from application to application, a plus-minus 25% margin of error is a good indication that the input values for Manning's and eddy viscosity are representing the real conditions. Figure 14 provides a comparison of the estimated versus measured depth averaged velocity. For about 15% of the calculated points the deviation exceeded the 25% threshold. There are several reasons for exceeding the threshold. One possible reason could be the built-in assumption in FESWMS that the flow follows the logarithmic law. Although this is true along the centerline of the channel where the flow does not experience a disturbance by the presence of the structures, the velocity profile deviates from the log law in the vicinity of the structures (Kironoto and Graf, 1987). Another reason for the wide scatter found in the velocity plots is the error between the measured and flow depth. This error propagates during the velocity measurements and magnifies the scatter between measured and estimated velocities (Pasternack et al., 2006). Finally, the LSPIV technique despite its advantages presents some inherent limitations. A recent study by Kim (2006) suggests that several parameters such as lighting, wind, and seeding contribute to an error in the measured velocity. The accumulated error in some cases can be higher than 30% (Kim, 2006). Subsequently, the scattering shown in the previous plots can be attributed unilaterally to both model and measuring errors.

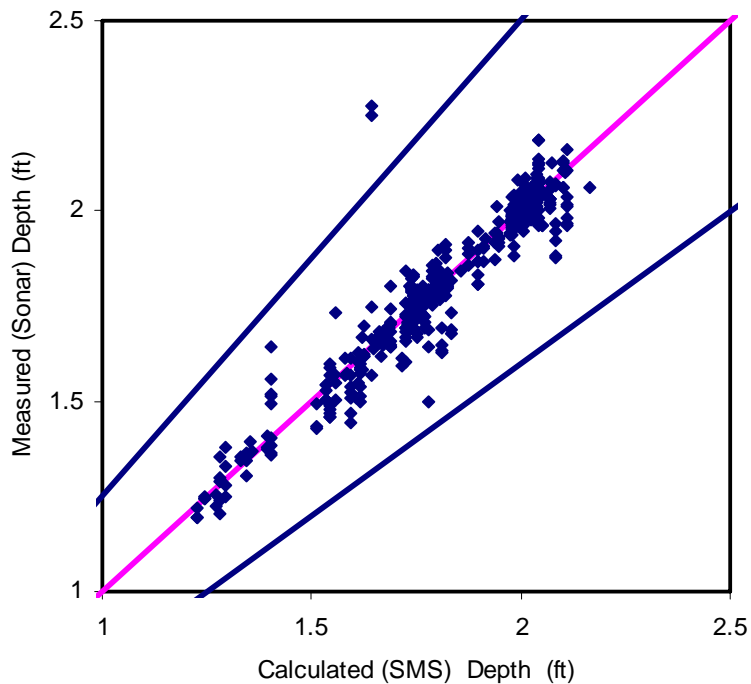


Figure 13. Comparison of calculated and measured depths.

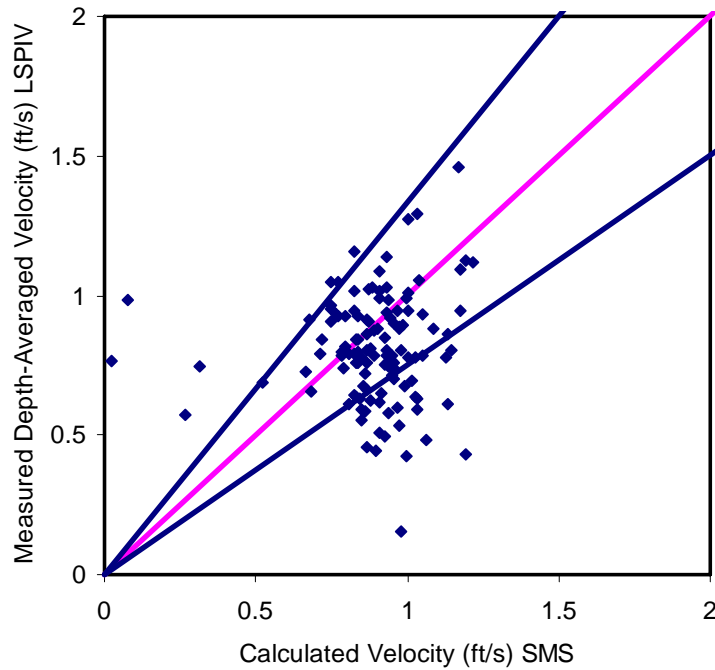


Figure 14. Comparison of calculated and measured velocities.

4.4 Calibrated Model

Five different eddy viscosity values were specified in the numerical code, the first one along the bank-line, the second one along the centerline of the recirculating flow, the third along the shear layer, the fourth one immediately behind the submerged portion of the bendway weir, and the fifth one on the flood plane area. Except for the undisturbed reach and the flood plane area, the Manning’s coefficient value in the region of interest (Figure 15) was set to 0.001. The Manning’s coefficient and eddy viscosity values for different locations within region of interest were summarized in Table 4.

Table 4: Manning’s coefficient and eddy viscosity for different locations.

Reach	Manning's n	Eddy viscosity
Undisturbed reach	0.055	0.06
Flood Plane	0.07	0.06
Areas with submerged barbs	0.001	0.06
Groyne Field	0.001	0.15
Shear layer	0.001	0.02
Turbulent behind weir	0.001	0.4
Banks	0.001	0.1

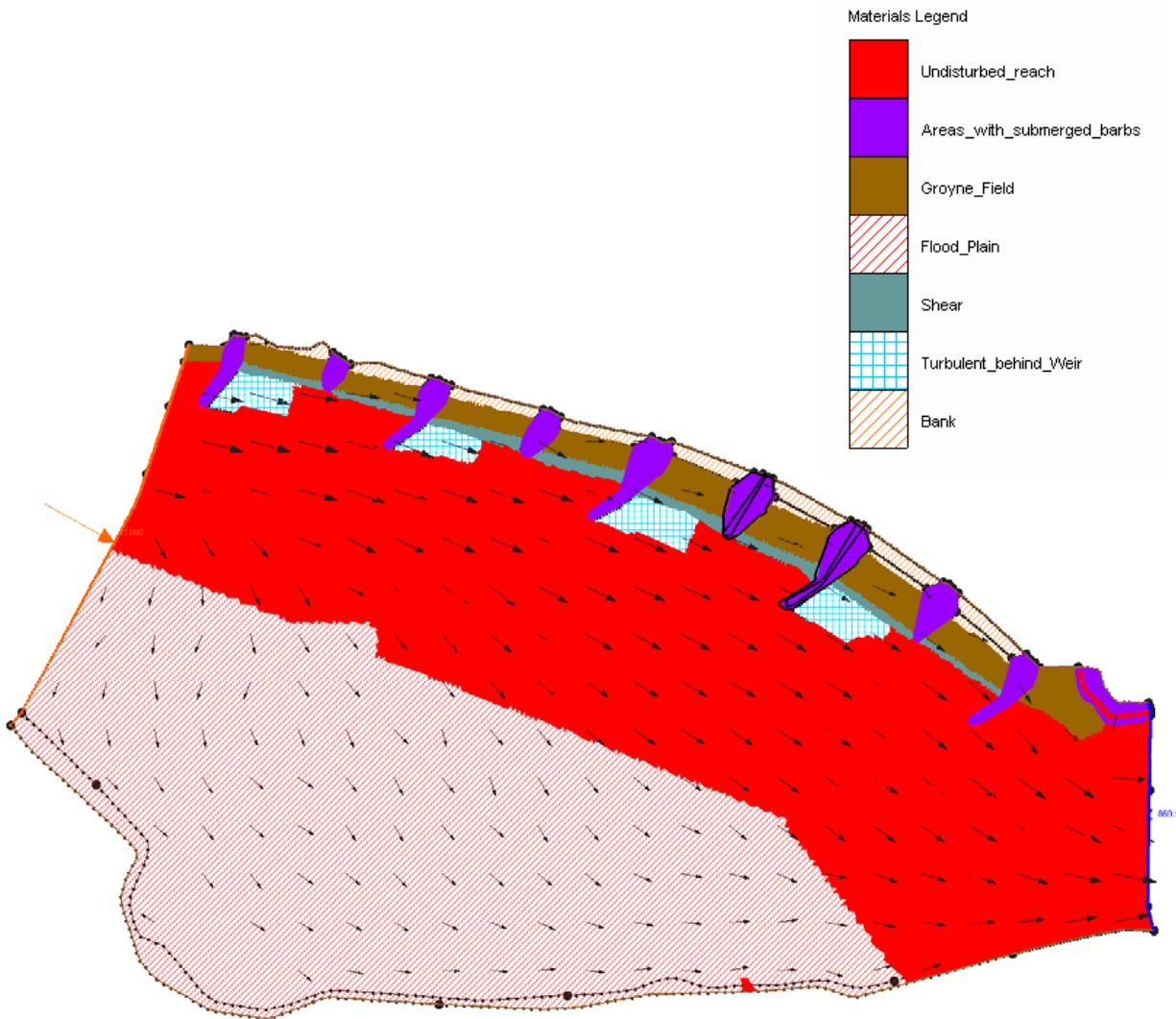


Figure 15. Classification of flow resistance areas according to Manning’s coefficient and eddy viscosity for the region of interest.

4.5 Sediment Transport Measurements

The flow measurements were complimented with general sediment transport measurements to identify the scour-hole and deposit pattern. Specifically, 22 points were inspected within the vicinity of the two furthest upstream structures during December 2006 and May 2007. The maximum deposition was found to be close to 2.5 ft, while the typical deposition was close to 1.0 ft. Deposition occurred between the structures and along the bank-line (Figure 16). Figure 17 provides a contour map with the depositional contour lines. As expected, scour was present around the toe of the structures and the scour depth varied between 3.0 ft to 9.0 ft (Figure 18). The above findings suggest that the river bed was active and therefore the assumption made in the model that the bed bathymetry remained unchanged was not true, and partly attributed to the wider scatter between the measured and estimated velocity values.

Sieve analysis of bed grab samples resulted to a d_{50} of 1.0 mm, d_{95} of 4.75 mm, and a d_{35} of 0.7 mm (Figure 19). For sand bed streams, the roughness height, k_s , is assumed to be well represented by the Engelund-Hansen formula, $k_s = 2d_{65}$ (van Rijn, 1982) where d_{65} was determined by the grain distribution.



Deposition area generated between barbs

Deposition along bank-line

Figure 16. Deposition processes after barbs construction.

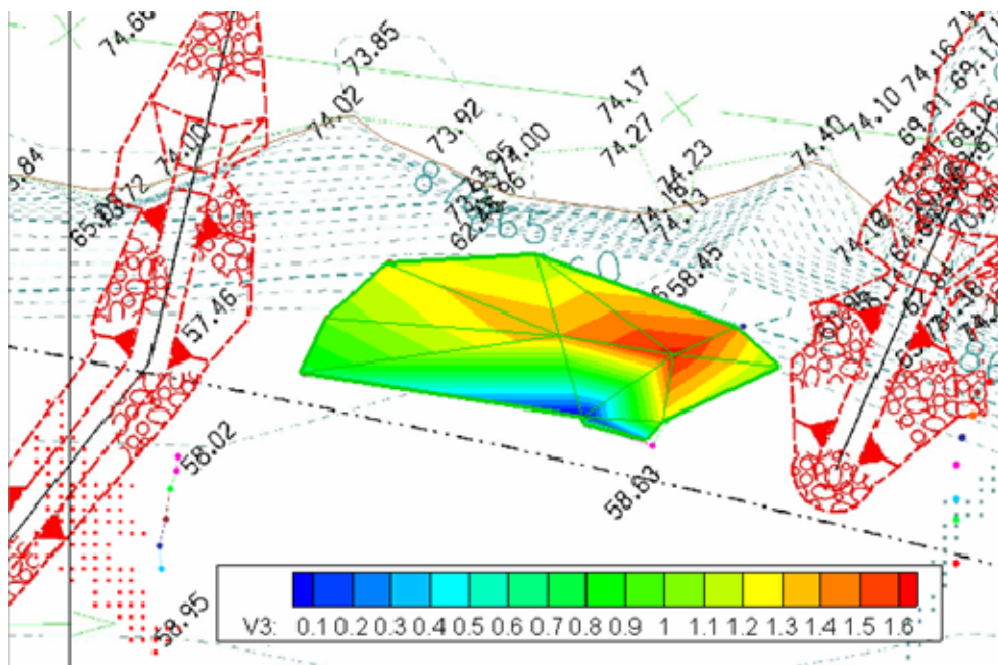


Figure 17. Measured deposition between two furthest upstream bendway weirs in ft.

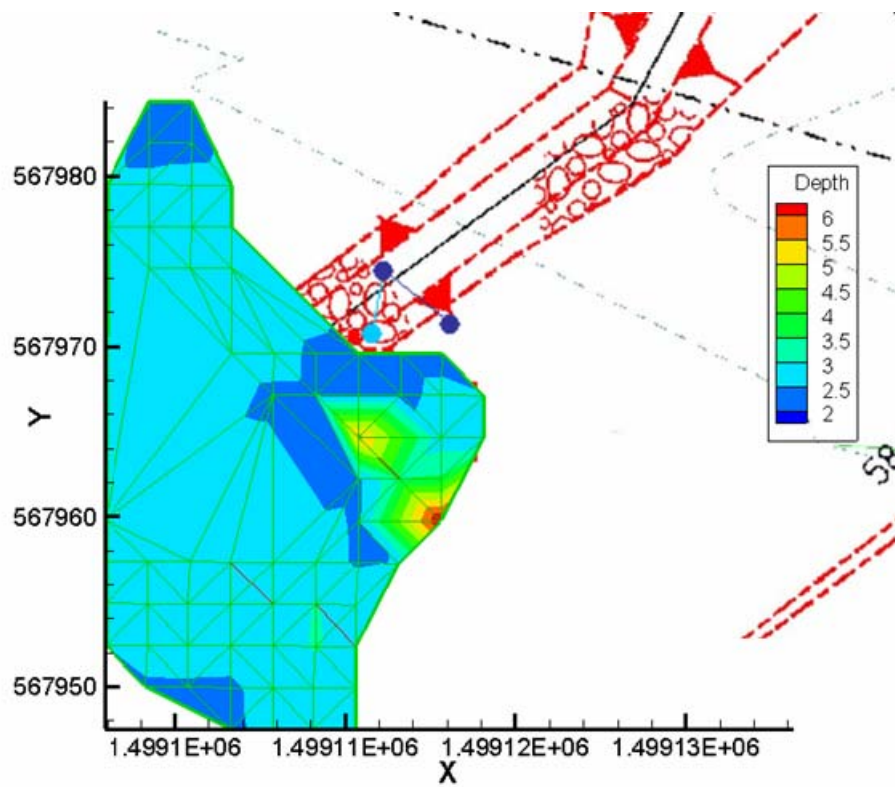


Figure 18. Measured scour depth around toe of bendway weir.

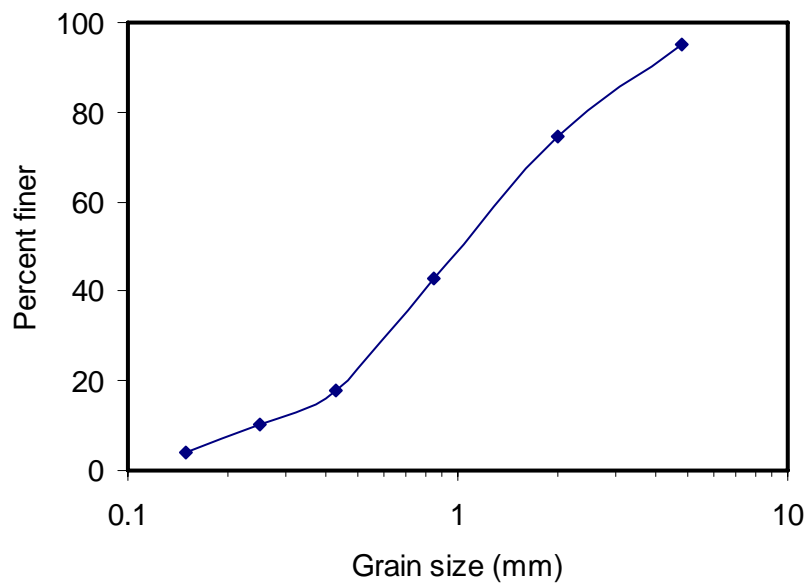


Figure 19. Sieve analysis of bed samples collected from the field site.

5. RESULTS

The hydraulic performance of the IDOT barbs design was examined using the calibrated model. To evaluate the barbs hydraulic performance in controlling bank erosion, the model was run for two conditions: first, in the pre-existing condition (i.e. before constructing the barbs); second, in the presence of the barbs. The model results for the pre-existing condition were used as a reference in comparing the model results in the presence of the barbs. The difference between the results was considered to be the effect of barbs on the site and used as a measure to their performance. Another factor that was investigated is the sand bar. Therefore, the model was run when the sand bar was present and when it was not present. One of the highest flow events ($Q = 11,000 \text{ ft}^3/\text{s}$, the bank-full condition) was considered in the analysis as described below.

Figures 20 to 23 comparatively illustrate the effects of the barbs on velocity, water depth, shear stress and the Froude number in the presence of the sand bar. The effects of the barbs on the same variables when the sand bar was not present are shown in Figures 24 to 27. The velocity and depth values obtained from the model simulations were used to calculate the shear stress and the Froude number. For each variable, the figures are designated as figures 'a' for the pre-existing condition and figures 'b' for the condition where the barbs present.

From Figures 20a and b, it is clear that the implementation of the barbs has dramatically decreased the velocities along the North bank of the channel and increased the velocities in the center of the channel. Figures 21a and b show comparisons between the flow depths. The miniscule changes in flow depth occurring with the addition of the barbs show very little, if any, backwater effects upstream. It can be assumed that because there are limited backwater effects, there will also be limited effects on the river upstream of the project area. Figures 20b and 21b show that deepest flows are located in areas where the velocity decelerates. This is an ideal situation for the incoming sediment transport to move and redistribute around the barbs and along the bank. The deceleration of flow in these region allow for sediment to settle. The above findings and explanations were confirmed with pictures taken at the site (Figure 16) for the deposited sediment between the barbs and along the bank. Similar trends were observed in the case when the sand bar does not present (Figures 24 and 25).

When comparing Figures 22a and b, it is evident that the barbs do aid in reducing the shear stress on the North bank, and when comparing Figures 23a and b, it can be seen that the barbs has decreased the Froude number along the North bank of the channel however very little increase can be observed in the Froude number near the center of the channel. Similar trends were observed in the case when the sand bar is not present (Figures 26 and 27).

In conclusion, the model results showed that the proposed design successfully reduced the flow velocity along the outside bank and increased the velocity towards the center of the stream, thereby successfully increasing the conveyance in the center of the channel. This means the spurs would be able to reduce the erosion along the North bank of the channel. It should be mentioned here that the produced velocities and shear stress values along the North bank in the present of the barbs are within the recommended values for channel stability design (Chaudhry, 1993). Removing the sand bar had minimum effects on the hydrodynamic processes occurring at the study site.

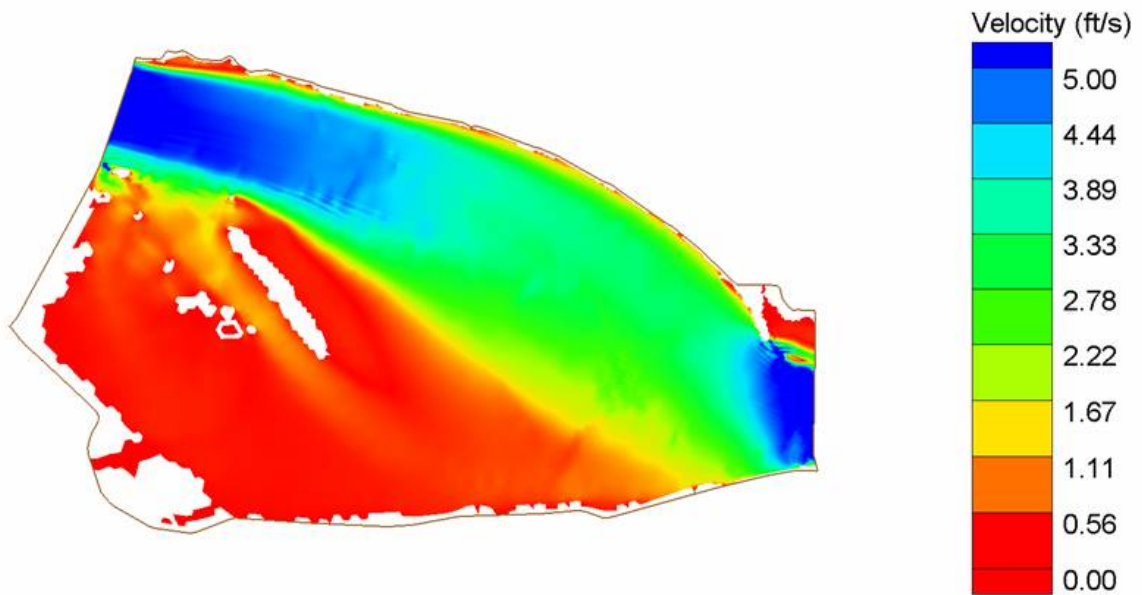


Figure 20a. No barbs present, sand bar present, discharge (Q) = 11,000 ft³/s, downstream water surface elevation (DWSE) = 869.9 ft.

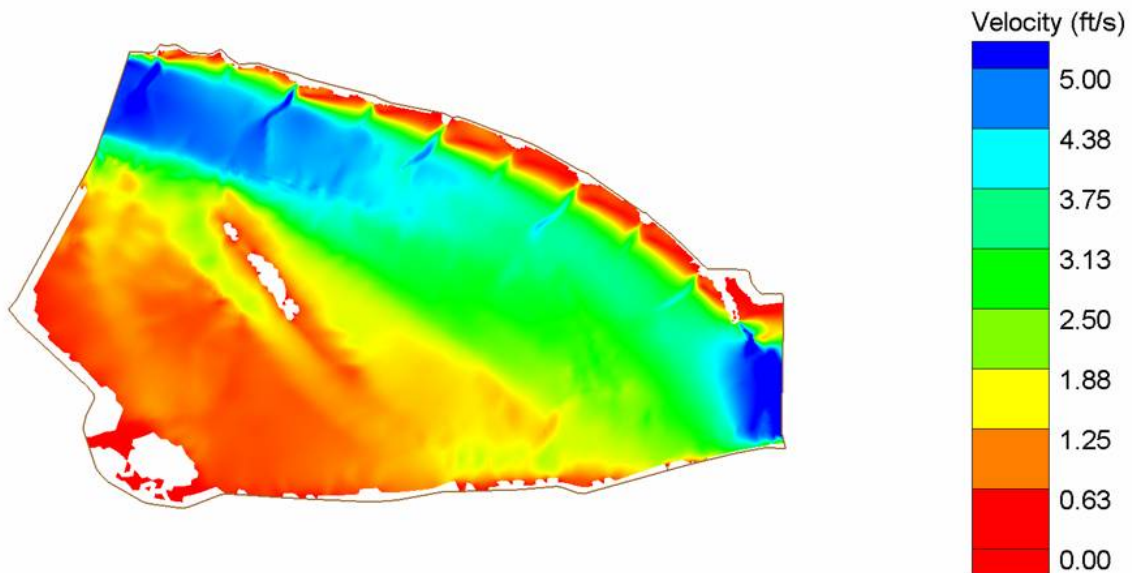


Figure 20b. Barbs present, sand bar present, discharge (Q) = 11,000 ft³/s, downstream water surface elevation (DWSE) = 869.9 ft.

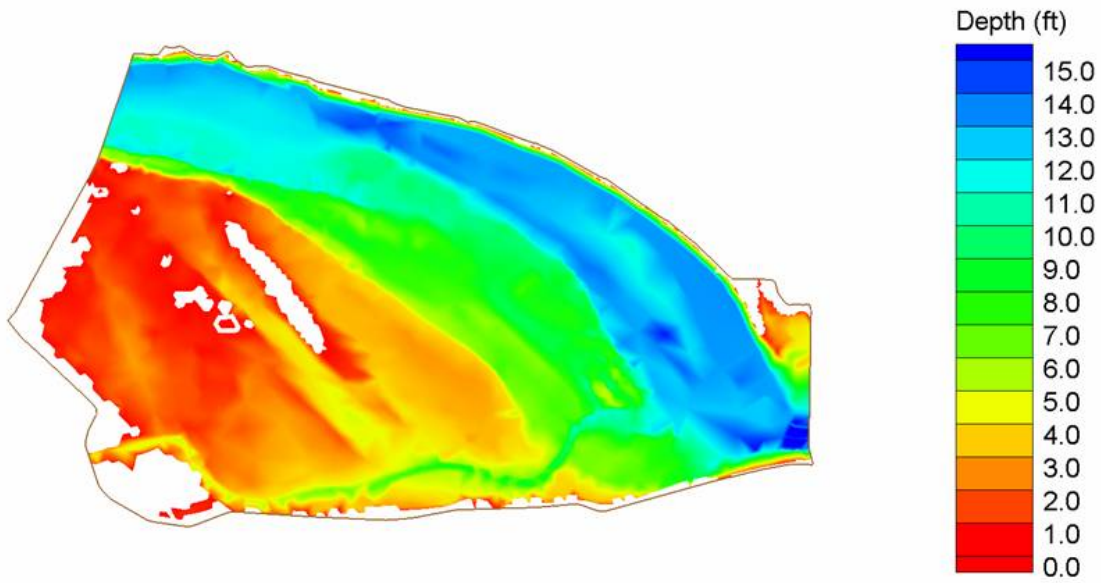


Figure 21a. No barbs present, sand bar present, discharge (Q) = 11,000 ft³/s, downstream water surface elevation (DWSE) = 869.9 ft.

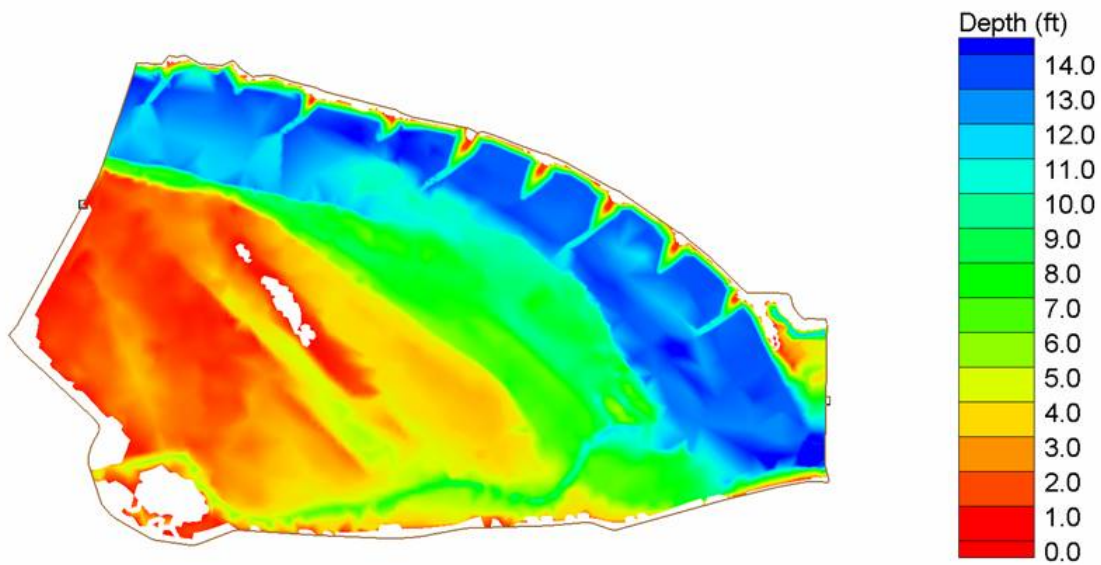


Figure 21b. Barbs present, sand bar present, discharge (Q) = 11,000 ft³/s, downstream water surface elevation (DWSE) = 869.9 ft.

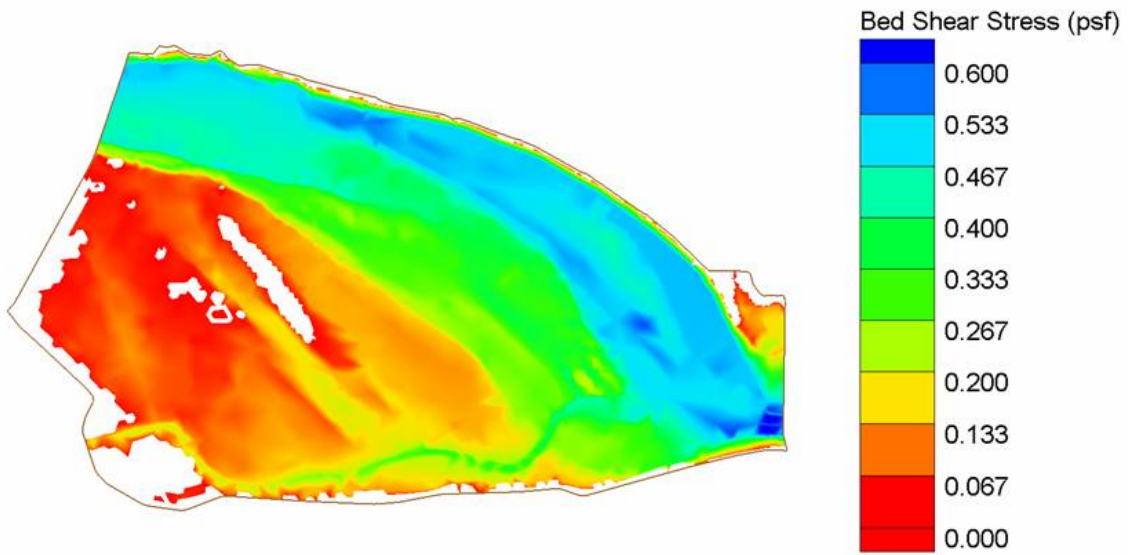


Figure 22a. No barbs present, sand bar present, discharge (Q) = 11,000 ft³/s, downstream water surface elevation (DWSE) = 869.9 ft.

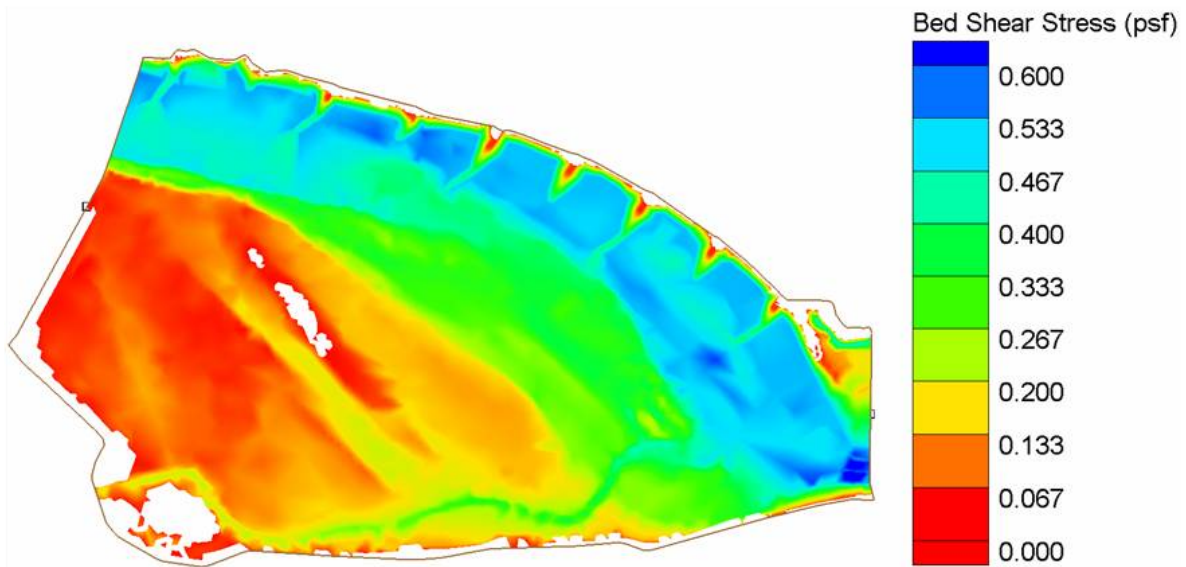


Figure 22b. Barbs present, sand bar present, discharge (Q) = 11,000 ft³/s, downstream water surface elevation (DWSE) = 869.9 ft.

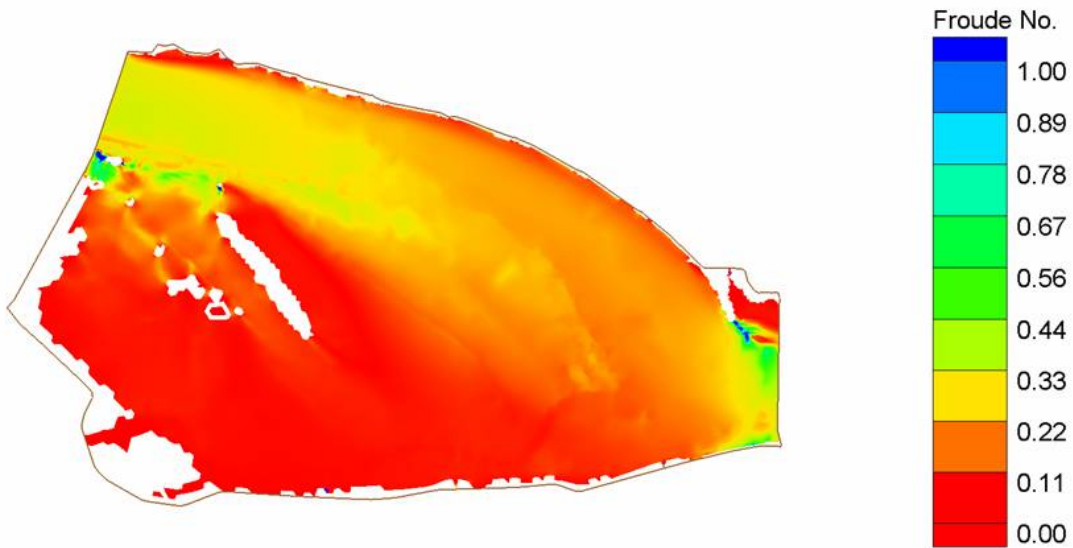


Figure 23a. No barbs present, sand bar present, discharge (Q) = 11,000 ft³/s, downstream water surface elevation (DWSE) = 869.9 ft.

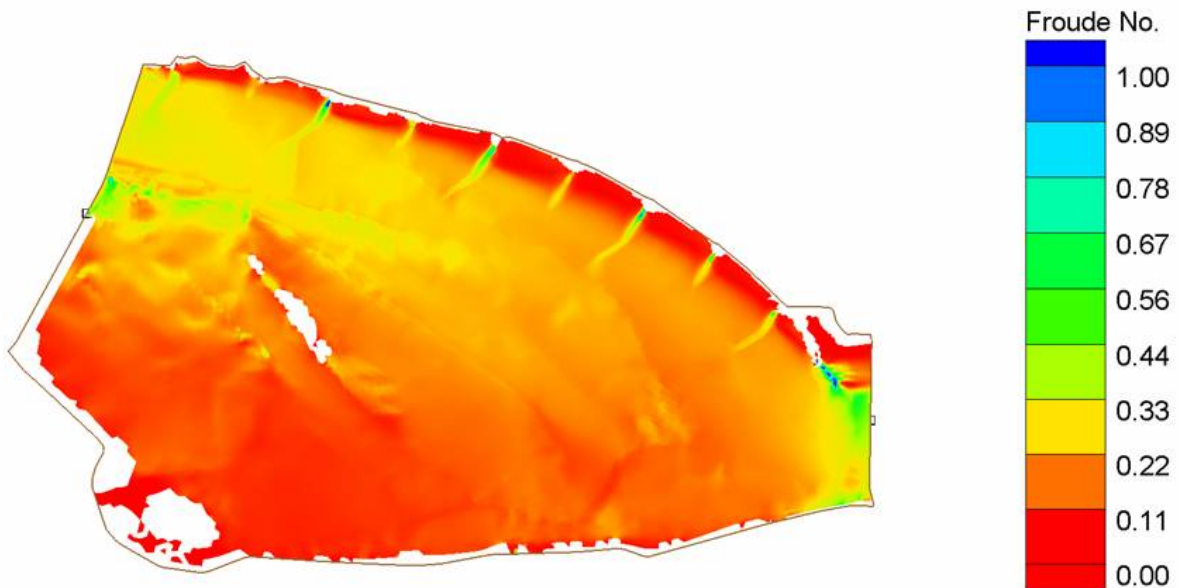


Figure 23b. Barbs present, sand bar present, discharge (Q) = 11,000 ft³/s, downstream water surface elevation (DWSE) = 869.9 ft.

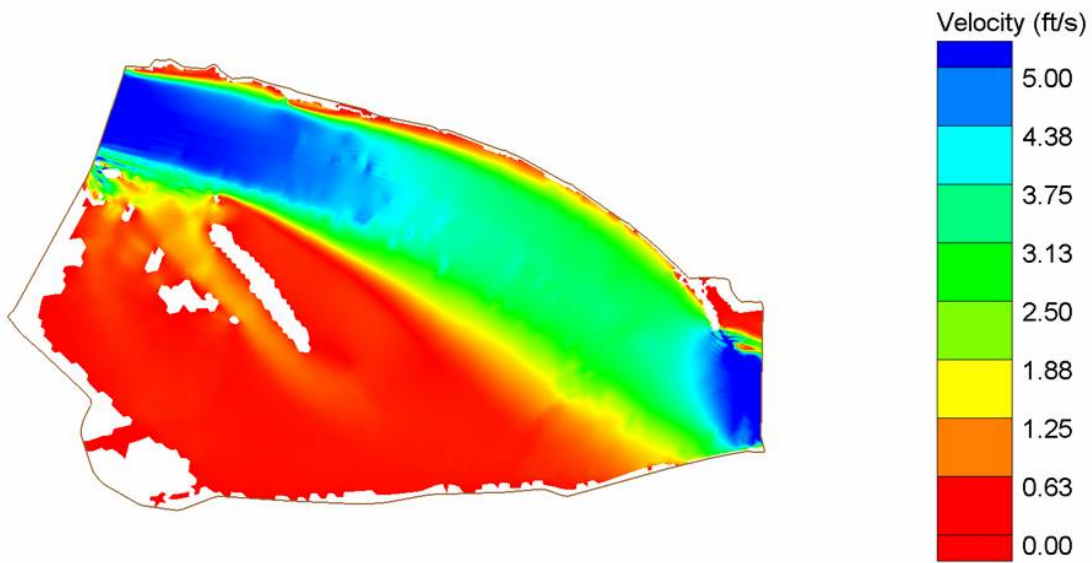


Figure 24a. No barbs present, no sand bar present, discharge (Q) = 11,000 ft³/s, downstream water surface elevation (DWSE) = 869.9 ft.

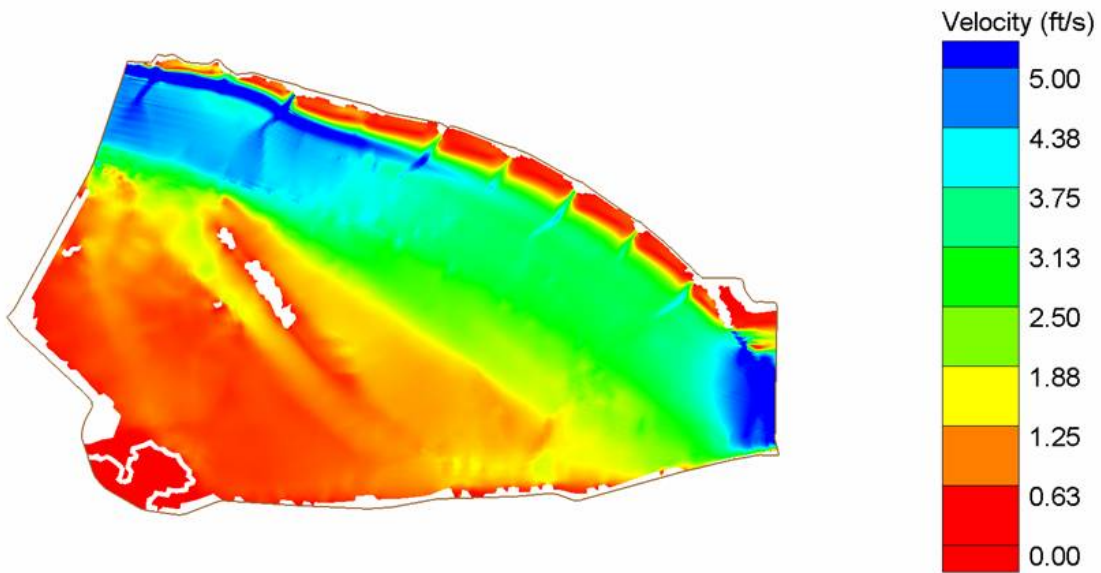


Figure 24b. Barbs present, no sand bar present, discharge (Q) = 11,000 ft³/s, downstream water surface elevation (DWSE) = 869.9 ft.

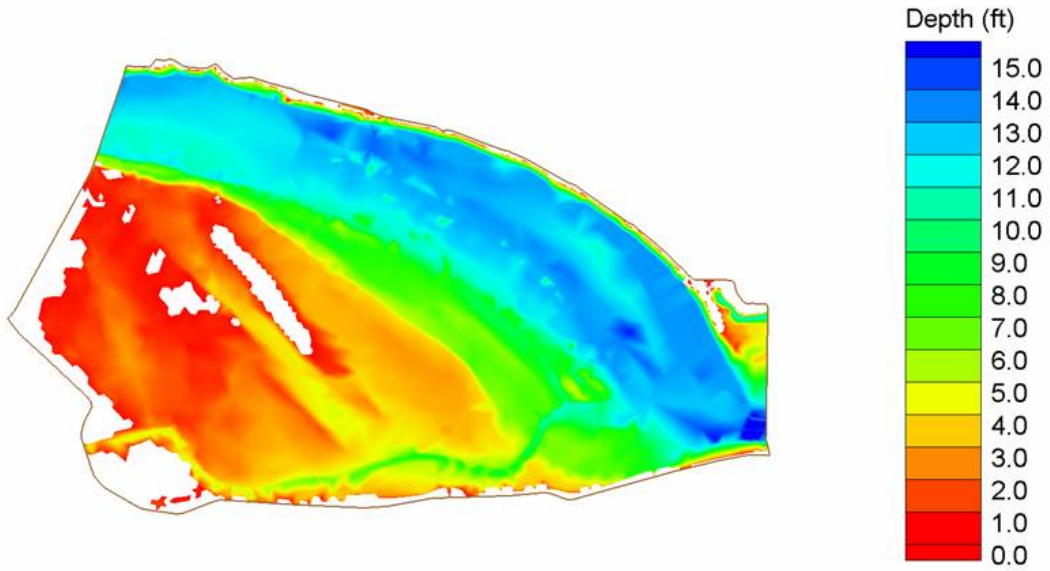


Figure 25a. No barbs present, no sand bar present, discharge (Q) = 11,000 ft^3/s , downstream water surface elevation (DWSE) = 869.9 ft.

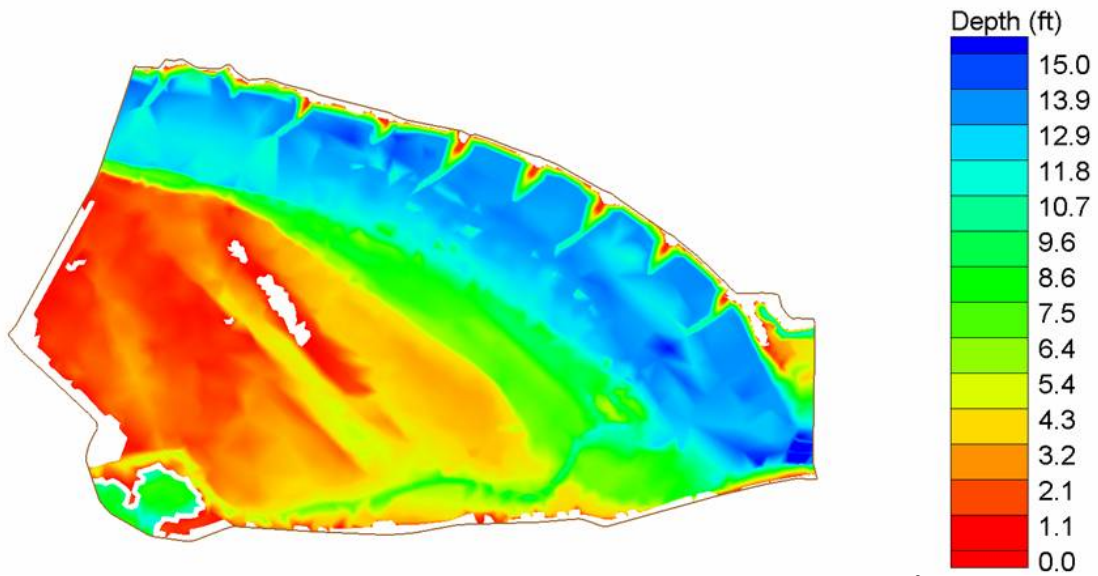


Figure 25b. Barbs present, no sand bar present, discharge (Q) = 11,000 ft^3/s , downstream water surface elevation (DWSE) = 869.9 ft.

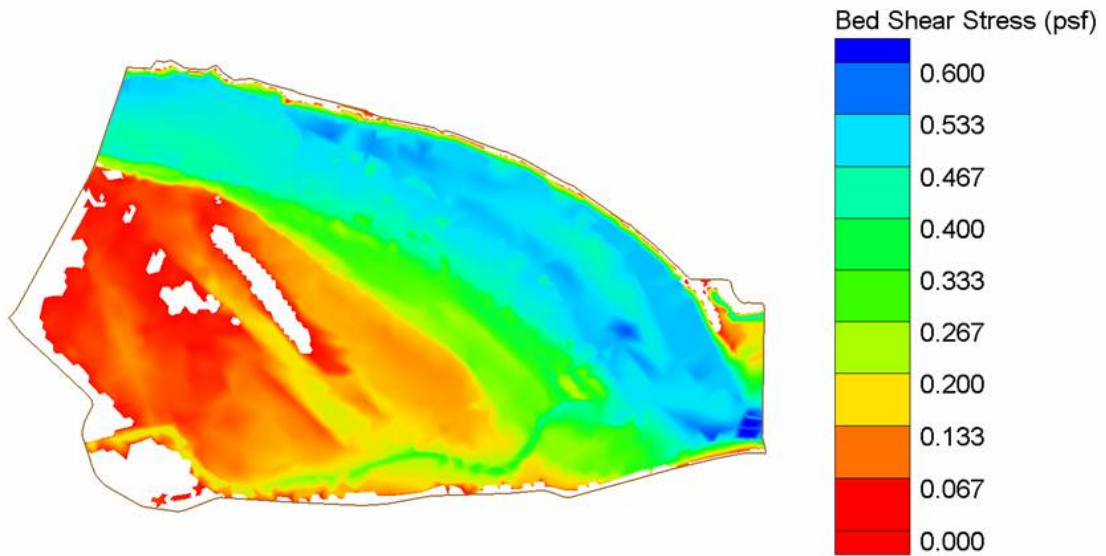


Figure 26a. No barbs present, no sand bar present, discharge (Q) = 11,000 ft³/s, downstream water surface elevation (DWSE) = 869.9 ft.

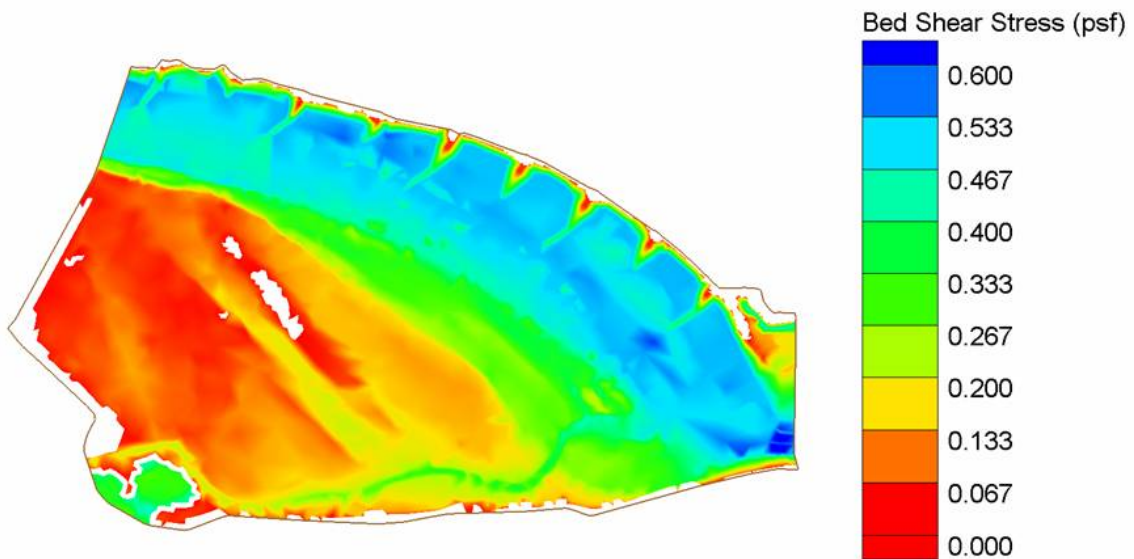


Figure 26b. Barbs present, no sand bar present, discharge (Q) = 11,000 ft³/s, downstream water surface elevation (DWSE) = 869.9 ft.

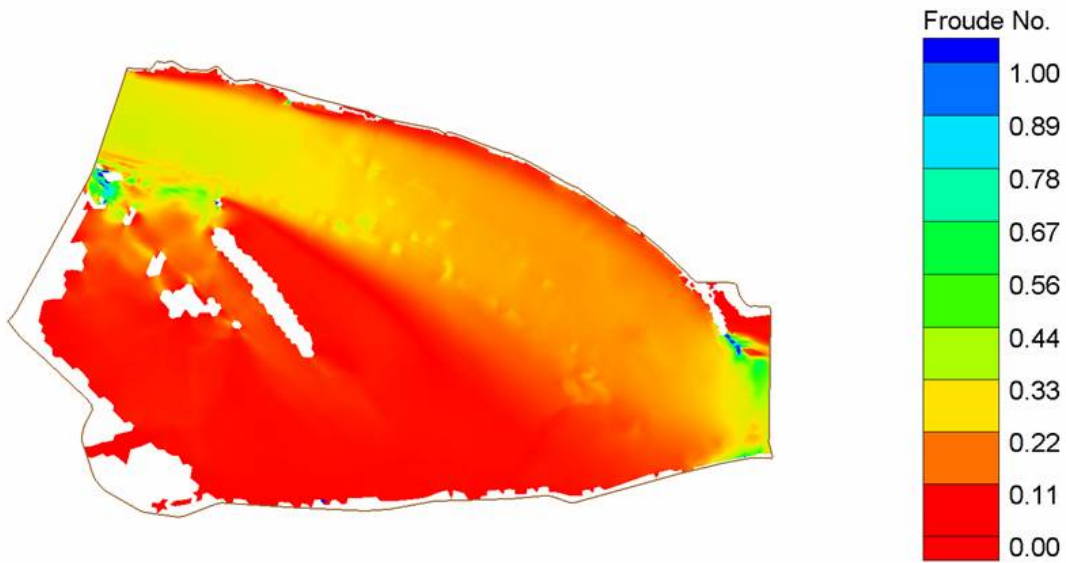


Figure 27a. No barbs present, no sand bar present, discharge (Q) = 11,000 ft³/s, downstream water surface elevation (DWSE) = 869.9 ft.

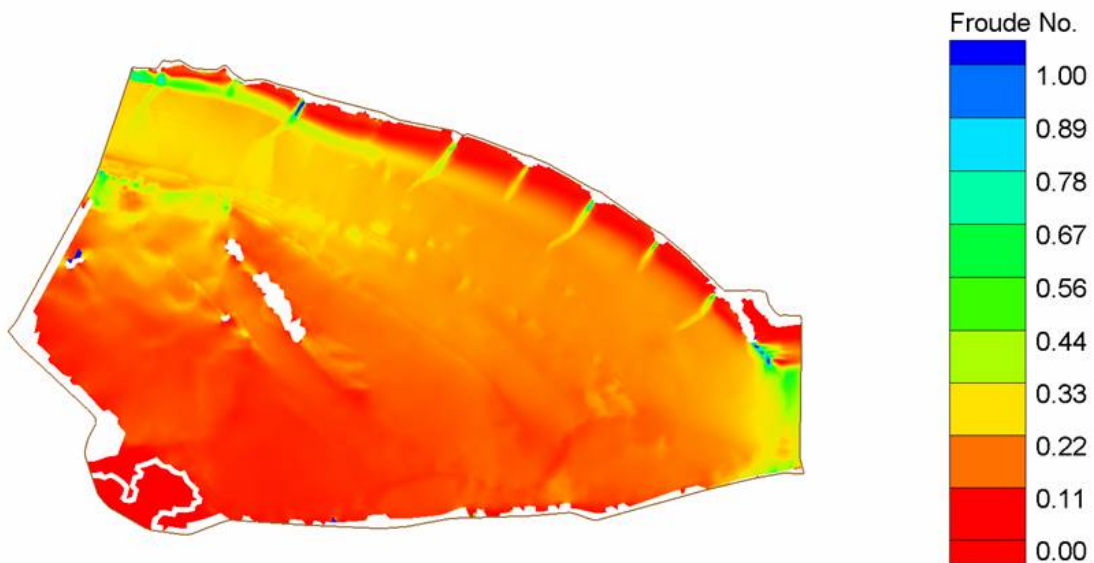


Figure 27b. Barbs present, no sand bar present, discharge (Q) = 11,000 ft³/s, downstream water surface elevation (DWSE) = 869.9 ft.

6. CONCLUSIONS

6.1 Numerical Model Performance

The commercially available two-dimensional, depth-averaged, hydrodynamic model FESWMS has proven to be a useful tool in both design and decision-making as it was able to adequately describe the interaction between the hydrodynamics of the flow in the channel system and the proposed bank erosion control structures. The model successfully predicts the flow patterns around submerged structures in a mild gradient sand bed river. A key factor for the success of the model in replicating the flow conditions after constructing the barbs was the detailed sensitivity analysis to isolate the effects of the Manning's coefficient and the eddy viscosity on the model output and the careful calibration of model. The calibration and verification of the model were made through detailed field measurements and a complete error analysis.

Flow measurements were conducted at the Raccoon River study site near Adel, Iowa. The field measurements were performed in two main regions in the channel, namely, the "external" region faraway from the barbs and near the center of the channel and the "internal" region in the close vicinity of the bendway weir. Cross-sectional velocity and depth measurements were performed via LSPIV and sonar recordings near the channel center to perform an "external" calibration of the average large scale flow processes occurring throughout the reach. A depth-averaged parabolic eddy viscosity value of $0.06 \text{ ft}^2/\text{s}$ was computed at the channel centerline and applied throughout the entire computational mesh during this exercise. An iterative trial and error process determined a Manning's coefficient value of 0.055 was necessary to match the calculated and measured depths within plus/minus 25%. The calculated measured and velocity magnitudes matched reasonably. LSPIV and detailed ADV flow measurements were also taken in close vicinity to the bendway weir to perform an "internal" calibration of the model. This internal calibration sought to provide a more detailed simulation of the local flow structure around the barbs. The ADV results provided a spatial representation of the varying eddy viscosity values around the structures. This was accounted for in the model by spatially refining the material properties around the structures. The model was then calibrated by comparing the resultant flow velocity magnitude to those measured by the LSPIV. This comparison was done along 20 transects in the wake region and it was determined the model adequately matches the velocity magnitudes and re-create the proper flow patterns.

Based on the model results, the proposed IDOT barbs design would be able to control bank erosion for most of the high flow events by reducing velocity magnitude along the channel bank and increasing conveyance in the center of the channel. The produced velocities and applied shear stress along the bank have been dropped to fall within the recommended values for channel stability design. Removing the sand bar had minimum effects on the hydrodynamic processes occurring at the study site.

In conclusion, a well calibrated two-dimensional, depth-averaged hydrodynamic model is a suitable tool for simulating flows around bendway weirs and evaluating their performance in mitigating bank erosion. The sensitivity analysis increases the user's knowledge on the effects of varying the individual input parameters and provides some insight into the model's uncertainty. The use of the detailed field measurements verify the models output and ensures that the models built-in assumptions, which although provide some inherent limitations, do not hinder the models overall capability to reproduce observed flow structure. Furthermore, the study expands the intended application of two-dimensional hydrodynamic numerical models by

demonstrating their capability in simulating averaged flow characteristics in highly turbulent regimes.

6.2 Structure Performance

First, it was found based on a 2 year monitoring and during bank-full flows that the maximum scour hole occurred away from the structures toe and the scour-hole size was directly related to the protrusion angle of the structure to the flow. Conventional angles of inclination analyzed throughout the literature include 45, 90 and 135 degrees. From the plethora of literature on this topic it has been concluded that the proposed structure inclination was appropriate since it provides maximum bank protection while creating the largest volume of local scour away from the structure and towards the center of the channel. Furthermore, the lowest potential for bank erosion also occurs with the present set-up design chosen by the IDOT.

Second, the riprap material incorporated into the structures (dikes and weirs) was directly and favorably correlated to the flow transmission through the structure, or in other words, dictated the permeable nature of the structure. An impermeable structure essentially deflects the current while a permeable structure slows down the current (Prezdwojski et al., 1995). In that line of thinking, it was found that the permeable dikes and weirs chosen in this study created less volume of scour in the vicinity of the structure toes and thus have less risk comparatively to other impermeable structures to collapse. The fact that the structures permitted the transmission of flow through them it allowed fine sand particles to fill in the gaps of the rock interstices and thus cement and better stabilize the structures. The design of structures was overall successful, including their spacing.

6.3 Environmental Benefits of Structures

Other benefits of employing riprap, as was the case here, include providing an environmentally oriented material with potential for ecological enhancement. As stated in the “Streambank Stabilization Handbook, (1998)” there is an intuitive feeling that structural restoration techniques, such as a group of spurs, brings many habitat improvements. These improvements include minimizing the effected streambed area, higher variability in bed topography forming resting pools, creating flow shade on the leeward side of the structure, and separation of bed substrate due to different flow conditions.

Another notable environmental benefit to rock riprap weirs and dikes is the creation of resting pools, especially in year 2007 (2nd year of the project). The magnitude of these benefits to aquatic habitat has been found in the literature that is directly related to the induced scour-hole volume (Kuhnle et al., 1999). Documented by Kuhnle et al. (1999), significant increases in fish size, numbers, biomass, and number of species was observed following the modification of spur dikes to increase scour-hole volume. We expect that this trend will be recorded in the study location.

Furthermore, the rocky surface of riprap material (typically conducive for growth of attachment type benthic macro-invertebrate species) provides a stable surface for benthic colonization which supplies food for aquatic organisms (Kuhnle et al., 1999).

REFERENCES

- Alvarez, J.A.M. (1989) Design of groins and spur dikes. In Proceedings of the 1989 National Conference on Hydraulic Engineering, ASCE, pp. 296-301.
- Bridge, J. S. (2004) *Rivers and Floodplains: Forms, Processes, and Sedimentary Record*, Blackwell, Malden, MA.
- Chaudhry, M.H. (1993). *Open Channel Flow*. Prentice Hall, Englewood Cliffs.
- Chen, F.Y., and Ikeda, S. (1997) "Horizontal separation flows in shallow open channels with spur dikes." *Journal of Hydroscience and Hydraulic Engineering*, 15 (2), 15-30.
- Claman, Dave, personal communication 2005.
- Cruetin, J.D., Muste, M., Bradley, A.A., Kim, S.C., and Kruger, A. (2003) "River gauging using PIV techniques: a proof of concept experiment on the Iowa River." *Journal of Hydrology*, Elsevier, 277, 182-194.
- Ettema, R. and Muste, M. (2004) "Scale effects in flume experiments on flow around a spur dike in flatbed channel." *Journal of Hydraulic Engineering*. 130 (7), 635-646.
- Fox J., Papanicolaou, A., Hobbs, B., Kramer, C., Kjos, L. (2005) "Fluid-sediment dynamics around a barb: an experimental case study of a hydraulic structure for the Pacific Northwest." *Canadian Journal of Civil Engineering*, NRC Canada, 32, 853-867.
- Froelich, D. (2002). *User's Manual for FESWMS Flo2DH: Two-Dimensional Depth-Averaged Flow and Sediment Transport Model, Release 3*.
- Hardy, R.J., Bates, P.D., Anderson, M.G. (1999) "The importance of spatial resolution in hydraulic models for floodplain." *Journal of Hydrology*, Elsevier, 216, 124-136.
- Hicks, D.M. and Mason, P.D. (1991). *Roughness Characteristics of New Zealand Rivers* New Zealand DSIR Marine and Freshwater Resources Survey, Wellington, NZ.
- Hobbs, B.W. (2005) *Two-dimensional numerical simulation of flow in a steep-gradient stream: implications for sediment transport and habitat conditions*. A Master's Thesis, University of Iowa, Iowa City.
- Khan, A.Z., Barkdoll, B. (2001) "Two-dimensional depth-averaged models for flow simulation in river bends." *International Journal of Computational Engineering Science*, 2 (3), 453-467.
- Kim, Y. (2006) *Uncertainty Analysis for Non-Intrusive Measurement of River Discharge Using Image Velocimetry*. A PhD Dissertation, University of Iowa, Iowa City.
- Kironoto, B. A. and W. H. Graf (1995) "Turbulence characteristics in rough non-uniform open-channel flow," Proc. Instn. Civ. Engrs. Wat., Marit. & Energy, Vol. 112, 336-348.
- Kuhnle, R. A., Alonso, C. A. and Shields Jr., F. D. (1999). "Geometry of scour holes associated with 90 degree spur dikes," *Journal of Hydraulic Engineering*, 125(9), 972-978.
- Lagasse, P.F., Schall, J.D., Johnson, F., Richardson, E.V., and Chang, F. (1995). *Stream stability at highway structures*. FHWA IP-90-014, HEC-20.
- Matin, H., Elbert, K.R. (2004) "Clackamette Cove-Clackamas Riverbank stabilization project A two dimensional element hydraulic model case study." *Proceedings of the 2001 ASCE Wetlands Engineering & River Restoration Conference, Reno, Nevada, August 27-31, 2001*.
- Mayerle, R., Toro, F.M., Wang, S.S.Y. (1994) "Verification of a three-dimensional numerical model simulation of the flow in the vicinity of spur dikes." *Journal of Hydraulic Research*, 33(2), 243-255.
- Melville, B.W., and Coleman, S.E. (2000) *Bridge Scour*. Water Resources Publications, Highlands Ranch, CO.

- Miller, A.J. and Cluer, B.L. (1998) "Modeling considerations for simulations of flow in bedrock channels." *Rivers over rock: Fluvial processes in bedrock channels*, AGU Monograph 107, AGU, Washington, D.C., 61-104.
- Papanicolaou, A.N. and Hildale, R. (2002) "Turbulence Characteristics in Gradual Channel Transition." *Journal of Engineering Mechanics*, 128 (9), 948-960.
- Pasternack, G.B., Gilbert, A.T., Wheaton, J.M., and Buckland, E.M. (2006) "Error propagation for velocity and shear stress prediction using 2D models for environmental management." *Journal of Hydrology*, Elsevier, 328 (1-2), 227-241.
- Przedwojski, B., Blazejewski, R., and Pilarczyk, K.W. (1995). *River Training Techniques*. A.A. Balkema, Rotterdam, Brookfield, Vt.
- Rajaratnam, N. and Nwachukwu, B.A. (1983) "Flow Near Groin-Like Structures." *Journal of Hydraulic Engineering*, 109 (3), 463-479.
- Schmidt, J.C., Rubin, D.M., and Ikeda, H. (1993) "Flume simulation of recirculating flow and sedimentation." *Water Resources Research*, AGU, 29, 2925-2939.
- Shields, F.D., Knight, S.S., and Cooper, C.M. (1998) "Addition of spurs to stone toe protection for warmwater habitat rehabilitation." *Journal of the American Water Resources Association*, 34 (6), 1427-1436.
- Streambank Stabilization Handbook (1998). Surface Armor for Erosion Protection, Chapter 7, U.S. Army Corps of Engineers and Veri-Tech Incorporated.
- Sukhodolov, A., Uijtewaal, W., and Englehardt, C. (2002) "On the correspondence between morphological and hydrodynamical patterns of groyne fields." *Earth Surface Processes and Landforms*, 27, 289-305
- van Rijn, L.C., "Equivalent Roughness of Alluvial Bed." *Journal of Hydrualic Div. ASCE*, 108(HY10), 1215-1218.

APPENDIX 1: External Calibration Results

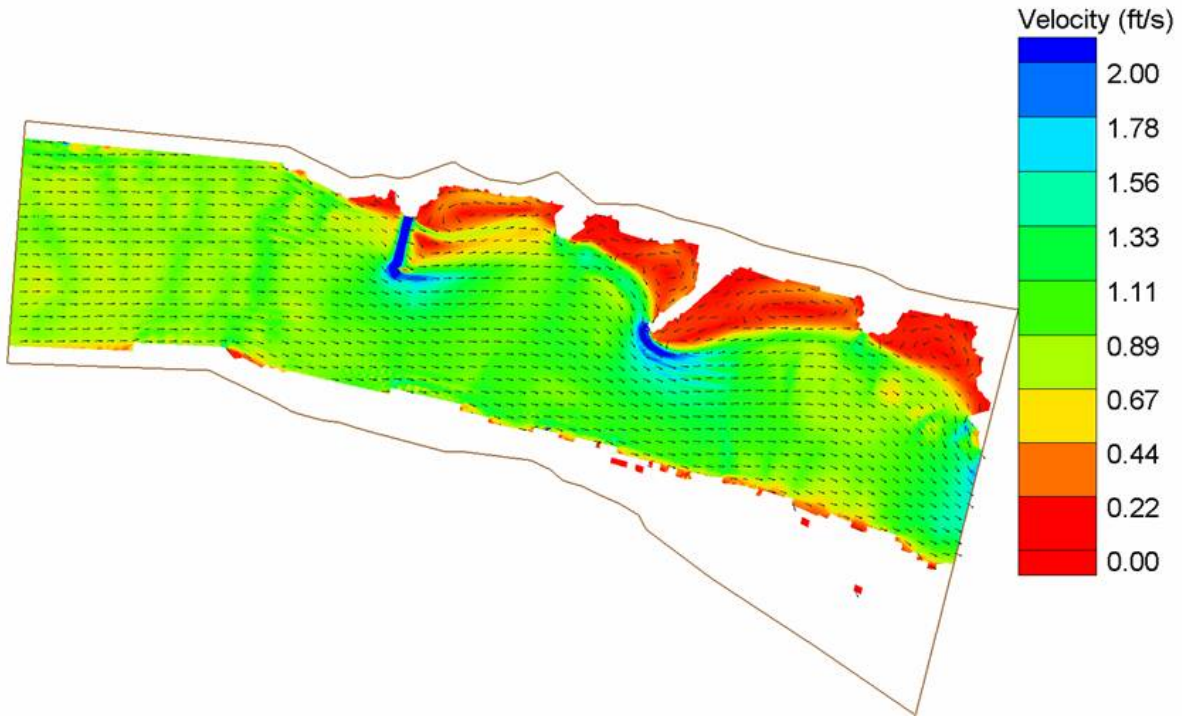


Figure A1. External calibration, discharge (Q) = 315 ft³/s, downstream water surface elevation (DWSE) = 861.38 ft.

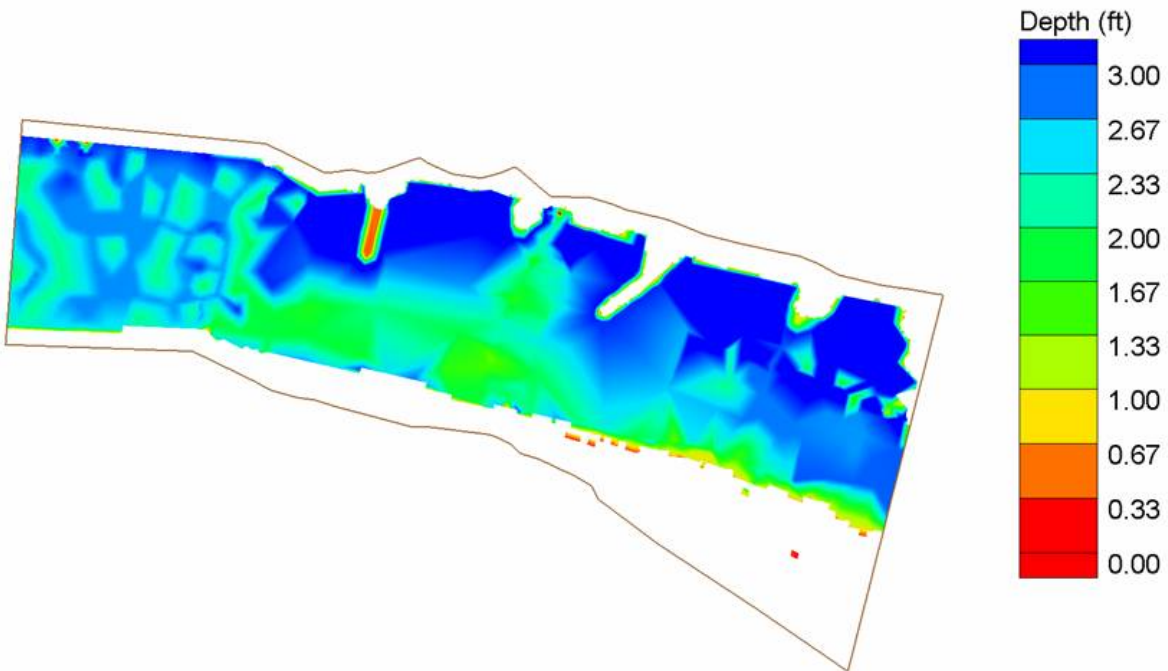


Figure A2. External calibration, discharge (Q) = 315 ft³/s, downstream water surface elevation (DWSE) = 861.38 ft.

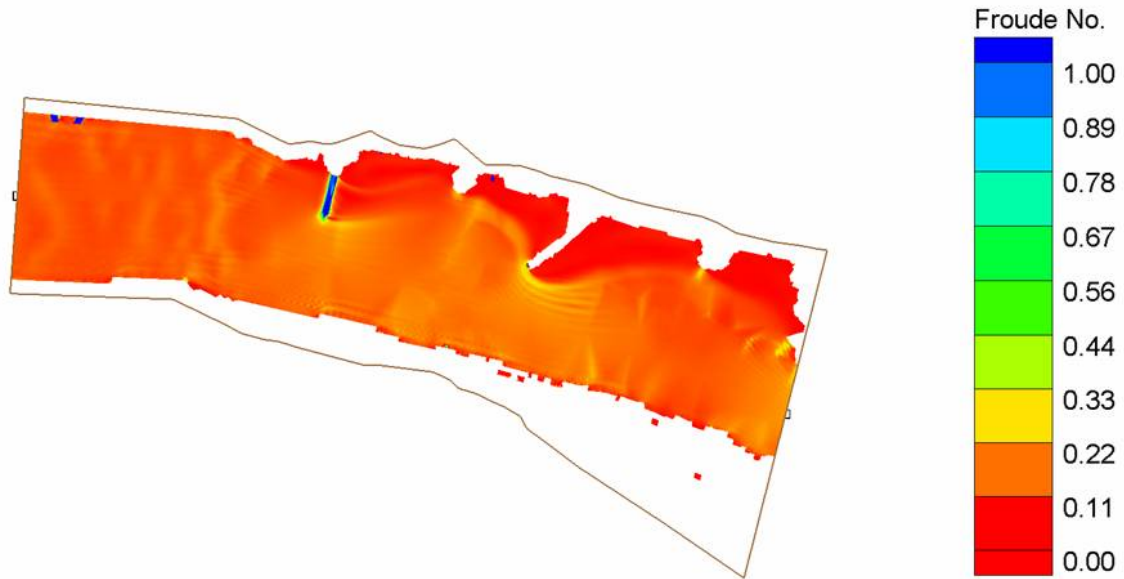


Figure A3. External calibration, discharge (Q) = 315 ft³/s, downstream water surface elevation (DWSE) = 861.38 ft.

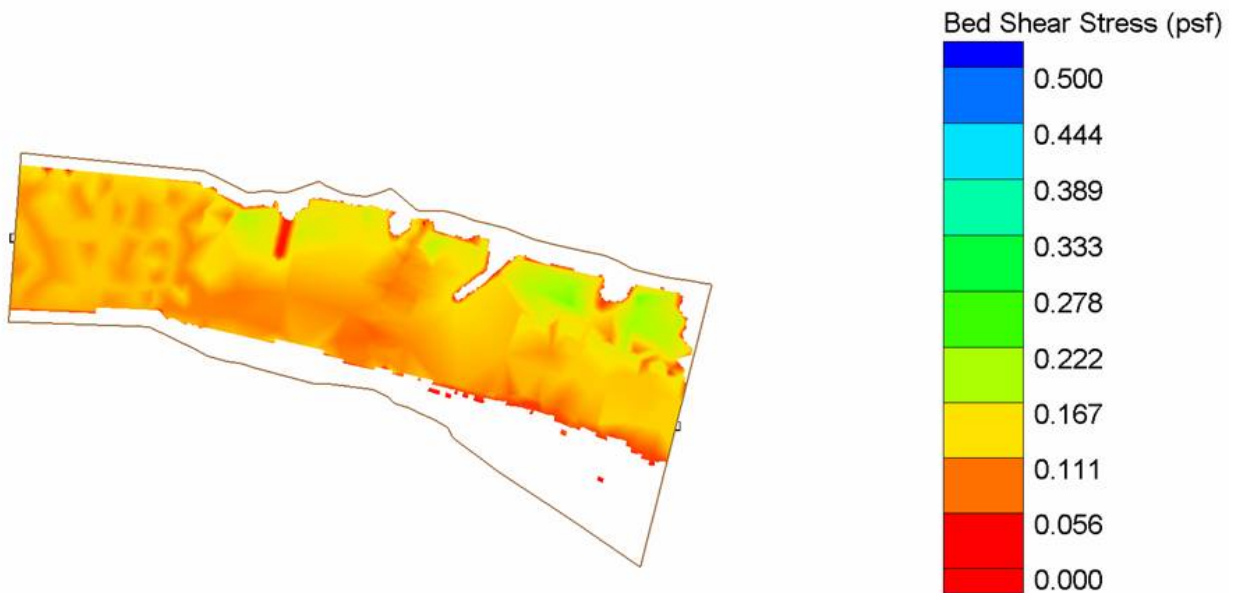


Figure A4. External calibration, discharge (Q) = 315 ft³/s, downstream water surface elevation (DWSE) = 861.38 ft.

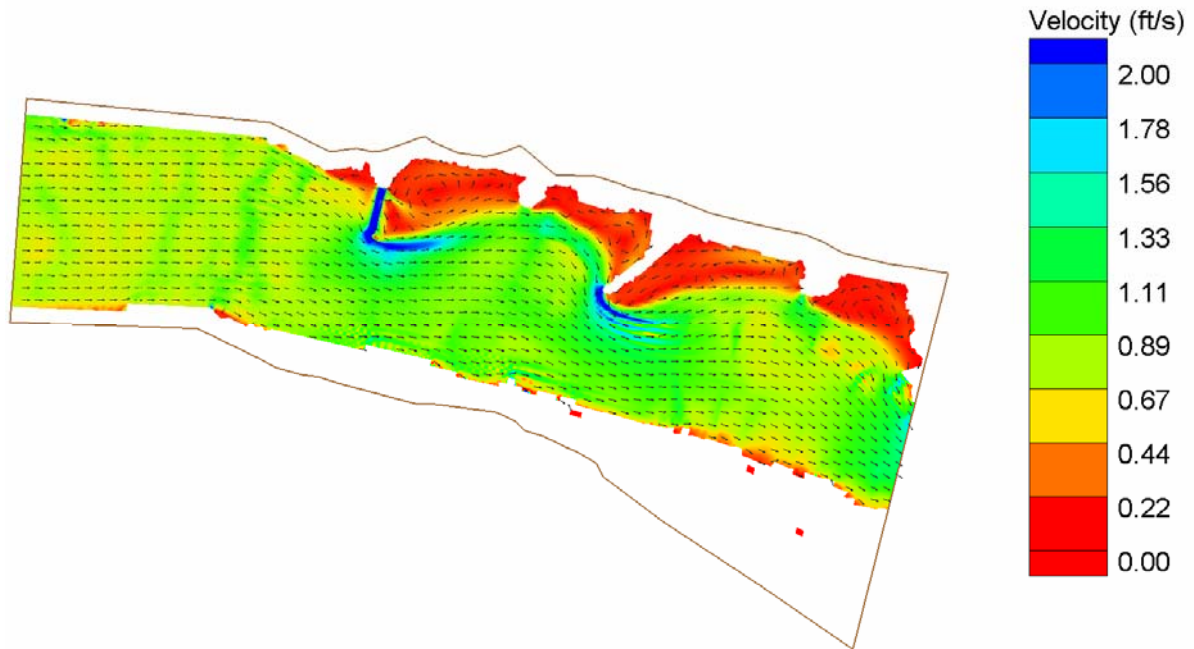


Figure A5. External calibration, discharge (Q) = 250 ft³/s, downstream water surface elevation (DWSE) = 861.15 ft.

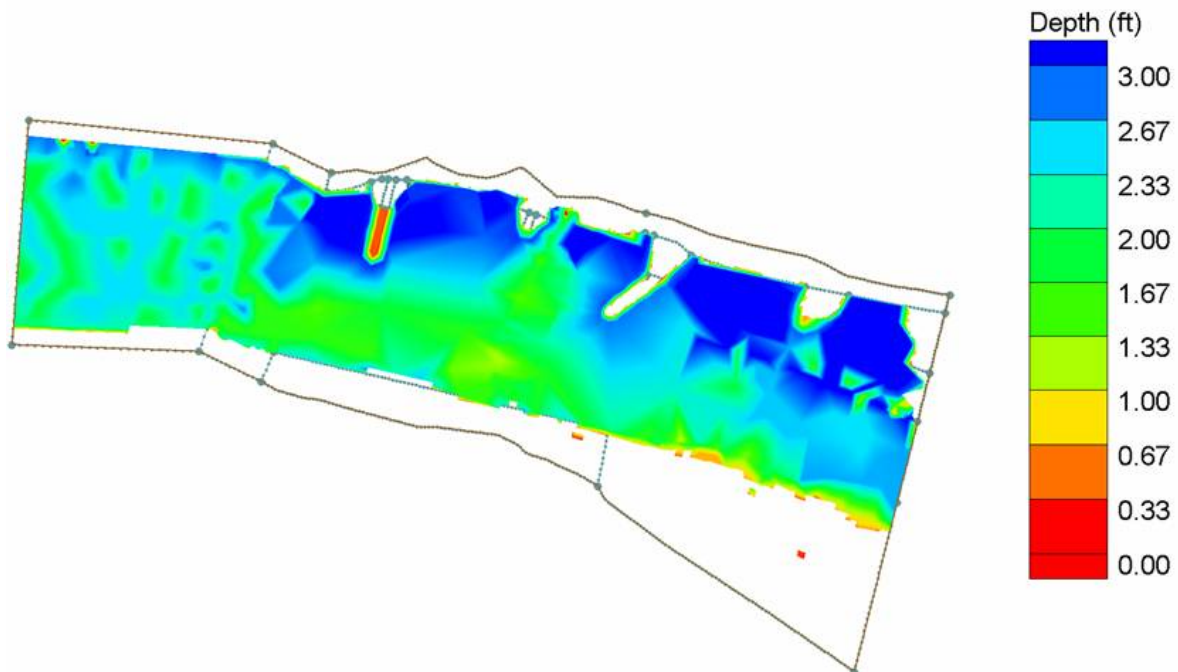


Figure A6. External calibration, discharge (Q) = 250 ft³/s, downstream water surface elevation (DWSE) = 861.15 ft.

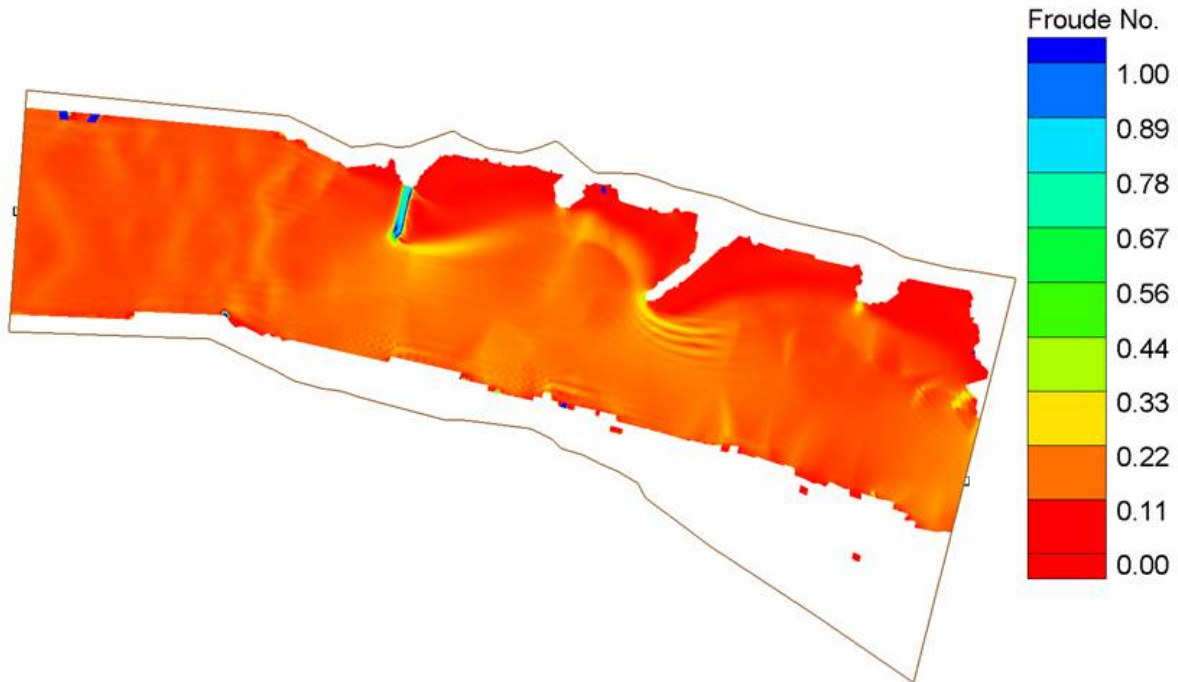


Figure A7. External calibration, discharge (Q) = 250 ft³/s, downstream water surface elevation (DWSE) = 861.15 ft.

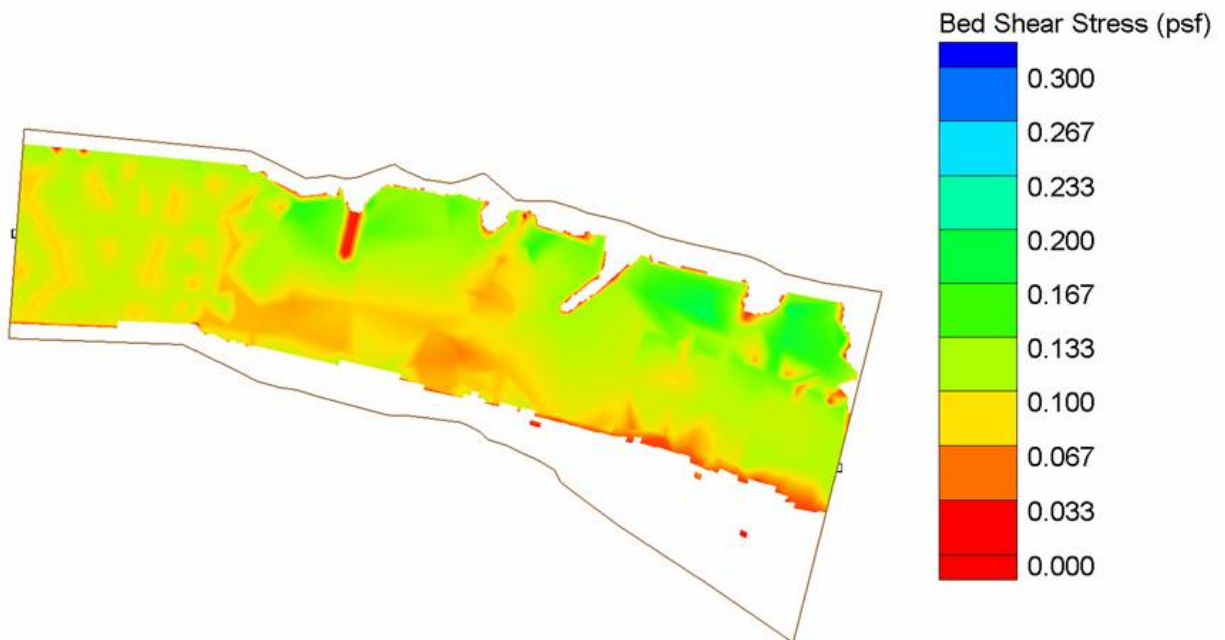


Figure A8. External calibration, discharge (Q) = 250 ft³/s, downstream water surface elevation (DWSE) = 861.15 ft.

